inorganics

MDPI

Review

Recent Progress of β-Ga_2O_3 Power Diodes: A Comprehensive Review

Lin-Qing Zhang [1,*], Jia-Jia Liu [1], Ya-Ting Tian [1], Han Xi [1], Qing-Hua Yue [1], Hong-Fang Li [1], Zhi-Yan Wu [1,*] and Li-Fang Sun [2]

[1] College of Electronic and Electrical Engineering, Henan Normal University, No. 46, East of Construction Road, Xinxiang 453007, China

[2] College of Information Engineering, Xinxiang Vocational and Technical College, No. 6, Jing San Road, Economic and Technological Development Zone, Xinxiang 453006, China

* Correspondence: 2017072@htu.edu.cn (L.-Q.Z.); 2018010@htu.edu.cn (Z.-Y.W.)

Abstract

Ultra-bandgap semiconductor material, β-gallium oxide (β-Ga_2O_3), has great potential for fabricating the next generation of high-temperature, high-voltage power devices due to its superior material properties and cost competitiveness. In addition, β-Ga_2O_3 has the advantages of high-quality, large-size, low-cost, and controllable doping, which can be realized by the melt method. It has a wide bandgap of 4.7–4.9 eV, a large breakdown field strength of 8 MV/cm, and a Baliga figure of merit (BFOM) as high as 3000, which is approximately 10 and 4 times that of SiC and GaN, respectively. These properties enable β-Ga_2O_3 to be strongly competitive in power diodes and metal-oxide-semiconductor field-effect transistor (MOSFET) applications. Most of the current research is focused on electrical characteristics of those devices, including breakdown voltage (V_{BR}), specific on-resistance ($R_{ON,SP}$), power figure of merit (PFOM), etc. Considering the rapid development of β-Ga_2O_3 diode technology, this review mainly introduces the research progress of different structures of β-Ga_2O_3 power diodes, including vertical and lateral structures with various advanced techniques. A detailed analysis of Ga_2O_3-based high-voltage power diodes is presented. This review will help our theoretical understanding of β-Ga_2O_3 power diodes as well as the development trends of β-Ga_2O_3 power application schemes.

Keywords: β-Ga_2O_3; power diodes; breakdown voltage; specific on-resistance

check for updates

Academic Editor: Hicham Idriss

Received: 3 September 2025

Revised: 17 October 2025

Accepted: 27 October 2025

Published: 31 October 2025

Citation: Zhang, L.-Q.; Liu, J.-J.; Tian, Y.-T.; Xi, H.; Yue, Q.-H.; Li, H.-F.; Wu, Z.-Y.; Sun, L.-F. Recent Progress of β-Ga_2O_3 Power Diodes: A Comprehensive Review. *Inorganics* **2025**, *13*, 364. https://doi.org/10.3390/inorganics13110364

1. Introduction

With the increasing need for high-power and high-voltage applications of electronic devices, Si cannot meet the requirements due to its narrow bandgap (E_g~1.12 eV). GaN (E_g~3.4 eV) and SiC (E_g~3.3 eV) power devices exhibit excellent breakdown properties, low conduction, and switching loss due to the higher electron mobility [1–3]. However, to obtain excellent quality crystals, these materials need epitaxial growth techniques, which result in high costs and restrict their application. Recently, Ga_2O_3, as a promising ultra-wide-bandgap semiconductor material, has gradually emerged, and it attracts extensive attention from the global scientific research community and industry [4–10]. β-Ga_2O_3, mostly thermally and chemically stable in five polymorphs (α, β, γ, δ, ε), has a wide bandgap of 4.6–4.9 eV, a large breakdown field strength of 8 MV/cm, and excellent Baliga figure and Johnson's figure of merit (JFOM). These properties make it a strong competitor as an alternative material for power devices. A comparison of important physical properties for commonly used semiconductor materials is shown in Table 1 [11,12].

Table 1. Important physical properties for commonly used power semiconductors.

Parameter	Si	GaAs	4H-SiC	GaN	Diamond	β-Ga_2O_3	AlN	h-BN	ZnO
E_g (eV)	1.12	1.43	3.2	3.4	5.5	4.7–4.9	6.2	6.1	3.37
M (cm^2/Vs)	1480	8400	1000	1250	2000	200–300	30	62	/
E_C (MV/cm)	0.3	0.4	2.5	3.3	10	8	15.4	7	0.01
V_S (10^7cm/s)	1	1.2	2	2.5–2.6	1	1.8–2	1.3	/	3.2
Thermal conductivity (WmK^{-1})	150	5	490	200	2200	23	319	625	50
Dielectric constant (ε)	11.8	12.9	9.7	9	5.5	10	9.76	4.97	8.5
BFOM	1	14.7	317	846	24,660	3214	32,384	3083	10
JFOM	1	1.8	278	1089	81,000	2844	7744	/	/

As can be seen in Table 1, SiC and GaN have high BFOM values, and their devices have developed rapidly in the past few years, with commercial applications such as electric vehicles and computer power supplies. However, these materials need epitaxial growth techniques, which result in high costs and restrict their application. In addition, GaN material has problems with p-type doping. In recent years, ultra-wide-bandgap (UWBG) materials Ga_2O_3, AlN, h-BN, and diamond have emerged as promising candidates for future power electronics and have made remarkable progress. Their large E_G properties enable a high voltage tolerance, high power capabilities, and a high potential for high voltage adaptability at low on-resistance. Diamond has superior performance in comparison, with a BFOM of 24,460. Chemical stability, radiation resistance, mechanical hardness, and a high BFOM of AlN make it an ideal material for operation in harsh environments and high-temperature stability, with relatively superior performance. However, for h-BN and diamond material, difficulties in growing techniques and doping within the bulk material have limited their application. AlN also faces technical challenges in epitaxial growth and well-controlled n-type and p-type doping. In comparison, Ga_2O_3 has excellent inherent material characteristics, easy n-type doping techniques, low-cost substrate growth, and epitaxial techniques. However, it is not suitable for all power applications due to its lower electron mobility and poorer thermal management ability. This makes Ga_2O_3 particularly suitable for devices that require high-voltage support at low frequencies, such as diodes. For JFOM, which shows potential in high-voltage and high-frequency applications, Ga_2O_3 is not superior, as compared to AlN, diamond. It is slightly better than SiC and GaN. In recent years, radio frequency (RF) Ga_2O_3 devices have also shown significant progress.

In view of the significance of Ga_2O_3 in terms of material properties and application prospects, as well as the many current challenges, this review will summarize the research progress of β-Ga_2O_3 power diodes up to 2025. Section 2 will introduce the Ga_2O_3 material. The interface between Ga_2O_3 and other materials will be discussed in Section 3. Section 4 will systematically introduce and discuss the detailed electrical characteristics of β-Ga_2O_3 power diodes with the different structures and techniques proposed in recent years. Comparisons of different structures and techniques are proposed and discussed. Section 5 summarizes the β-Ga_2O_3 power applications and outlooks. The aim is to provide meaningful guidance to promote the further development of Ga_2O_3 materials and device technologies for researchers and industrial practitioners in related fields, accelerating β-Ga_2O_3 power devices' progress from laboratory to industrial applications.

2. Ga_2O_3 Materials

The β-Ga_2O_3 bulk single-crystal substrate growth methods include Czochralski (CZ), Edge-defined film-fed (EFG), Bridgman (vertical, VB), and floating zone (FZ) techniques [13–22]. To obtain large-scale β-Ga_2O_3 wafers with a large size and low defect density, the EFG and CZ methods are more promising. Up to now, Novel Crystal Technology in Japan has achieved the commercialization of melt-grown 6-inch β-Ga_2O_3 substrates. In addition, a high-quality n-type doping β-Ga_2O_3 epilayer can be realized using MOCVD, MBE, PLD, HVPE, and MOVPE methods by using Si, Ge, and Sn [23–30].

Due to its intrinsic properties, including deep acceptor levels, low valence band position, and high ionization energy, the p-type doping with high conductivity is difficult [31–35]. Calculations demonstrate the absence of shallow acceptors in Ga_2O_3, and holes exhibit self-trapping effects within the material [36,37]. Despite these difficulties, some efforts have been made for the p-type doping realization. For instance, in 2024, Zhu et al. [38] demonstrated p-type behavior in Cu-doped Ga_2O_3 nanoarrays. In addition, β-Ga_2O_3 is inclined to accept donor doping, such as with Mg or N, which always introduces deep acceptor states [39,40]. However, in bulk material, this has not yet resulted in efficient p-type conductivity.

Ga_2O_3 has five polycrystalline states, α, β, γ, κ (ε), and δ. For optical properties (β-Ga_2O_3), in 2025, Labed et al. [41] significantly reduced the density of interfacial states and suppressed Fermi energy level pinning by inserting a graphene monolayer into a W/β-Ga_2O_3 Schottky contact, which resulted in a deep-ultraviolet photodiode with a responsivity up to 14.49 A/W and an external quantum efficiency (EQE) of 7044%. In 2024, Zhang et al. [42] prepared β-Ga_2O_3 extreme ultraviolet photodetectors with a vertical Schottky barrier structure, resulting in a responsivity of 55.31 mA/W and EQE of 508% at 0 V bias, fast response, and stable operation from −193 to 100 °C, better than silicon-based detectors. In 2025, Fang et al. [43] improved Ni/β-Ga_2O_3 vertical Schottky barrier diode interface quality by surface treatment, realizing a high-performance day-blind UV detector with a low 12 fA dark current, 4.92×10^7 light-to-dark current ratio, 2.76×10^{15} Jones detectivity, and millisecond response.

κ-Ga_2O_3, also known as ε-Ga_2O_3, is the second most stable phase of Ga_2O_3, which can only be grown by heterogeneous epitaxy [44,45]. ε-Ga_2O_3 has mostly deep-energy-level internal impurities, which results in lower dark-state currents, making it more suitable for photodetectors. Thus, most of the reported ε-Ga_2O_3 photodetectors are metal–semiconductor–metal (MSM) type, which have simpler structures and easier fabrication processes. Similar to that reported for β-Ga_2O_3, the photodetection performance of ε-Ga_2O_3 varies greatly in different research results. The responsivity ranges from a few hundred mA/W to more than 10^4 A/W. The light-to-dark current ratio changes from 10^3 to 10^8. The detection capability and response time also show several orders of magnitude difference [46–52]. For instance, in 2025, Yang et al. [53] proposed ε-Ga_2O_3 thin films on a 2-inch sapphire substrate using off-axis pulsed laser deposition, with inhomogeneity of key parameters such as thickness and crystalline quality below 5%. Based on this 10×10 photodetector array, the responsivity at 240 nm under 20 V bias voltage reaches 52.77 A/W, the UV-visible suppression ratio is 1.2×10^4, and the photocurrent deviation of the array unit is ≤8%, providing a feasible solution for the use of wafer-scale Ga_2O_3 devices for high-quality imaging. In 2022, Chen et al. [54] grew high-quality ε-Ga_2O_3 thin films on sapphire and silicon substrates using metal-organic chemical vapor deposition (MOCVD). The ε-Ga_2O_3-based SAW piezoelectric resonators were demonstrated for the first time, with the devices resonating in Rayleigh and Sezawa modes in the ≈1–3 GHz range. Based on these results, the team proposed ε-Ga_2O_3 as a favorable piezoelectric semiconductor for 5G RF filters. In 2025, Zhang et al. [55] demonstrated a heterojunction design based on ultra-wideband semiconductors by integrating p-type diamond with n-type ε-Ga_2O_3 to prepare a p-n diode with a V_{BR} of more than 3000 V. The p-n diode is a heterojunction design based on an ultra-wideband semiconductor. Highly efficient rectifying heterojunctions were realized by pulsed laser deposition of heteroepitaxial ε-Ga_2O_3 thin films on a diamond substrate to form atomically sharp interfaces with C-O-Ga bonding. The devices have a switching ratio of more than 10^8, a turn-on voltage of about 2.5 V, and a high thermal boundary conductance of 42–64 $MW/m^2 \cdot K$. Numerical simulations show that lightly doped diamond as a drift layer combined with ε-Ga_2O_3 can effectively mitigate the electric field concentration effect and avoid premature breakdown. The design provides a feasible path for the application of ultra-wideband semiconductors in high-power bipolar devices. In addition, in 2022, Hidouri et al. [56] studied the carrier localization phenomenon of nominally undoped ε-Ga_2O_3 films deposited on (0001)-Al_2O_3 substrates by metal-organic vapor phase epitaxy using different O and Ga precursor ratios. The results can be very useful in enabling further development of Ga_2O_3 materials and related devices.

Among its polycrystalline states, the amorphous α-Ga_2O_3 is known for its low-cost preparation, low-temperature processing, and high efficiency. Because of the low carrier mobility and high defect density of α-Ga_2O_3, researchers are mainly focused on achieving performance breakthroughs through different modification strategies to provide technological support for the practical applications of day-blind ultraviolet detection (flexible electronics, space communication, and weak-signal detection). In 2025, Huang et al. [57] applied α-Ga_2O_3 and Mg:ZnO heterointerfaces for the first time to phototransistors, demonstrating improved separation, transport, and collection of photogenerated carriers with the excellent electron transport properties of Mg:ZnO. The resulting phototransistors have high photoresponsivity up to 1.27 A/W and a very thin photosensitive layer (~60 nm) with x-ray detection capability. In 2025, Xue et al. [58] used pulsed sputtering deposition to prepare α-Ga_2O_3 thin films on polyimide substrates. After rapid thermal annealing with H_2, the flexible day-blind photodetectors achieved a 222.98 A/W ultra-high response rate, a 9.49×10^5 high suppression ratio, and a 0.43/0.4 s fast response time, bending 500 times with a photocurrent stabilization rate of more than 90%, demonstrating the imaging sensor arrays and space light source detection applications.

The band gap and conduction band energy levels of γ-Ga_2O_3 are 4.65 eV and −1.12 eV, respectively, corresponding to conduction band potentials and valence band potentials of −3.38 V and +1.97 V, which are much more negative than the reduction potential of water ($H+/H_2$) and much more positive than the oxidation potential of water (O_2/H_2O). Therefore, γ-Ga_2O_3, as a broad-band semiconductor, satisfies the thermodynamic requirements for many reactions under UV irradiation. For example, GCN γ-Ga_2O_3 can be used for photocatalytic dinitrogen fixation and pollutant decomposition. γ-Ga_2O_3 also exhibits photocatalytic activity. However, the photocatalytic efficiency of γ-Ga_2O_3 is not as high as expected due to the short lifetime of photogenerated electrons and holes. It can only be applied under UV irradiation, which makes its photocatalytic applications extremely limited. In 2022, Huang et al. [59] used an electrostatic self-assembly method to prepare Ni_2P/γ-Ga_2O_3 nanosheet composites, and the yield of H_2 in pure water under UV light was up to 2.7 mmol g^{-1} h^{-1} and up to 12 mmol g^{-1} h^{-1} in methanol aqueous solution. Ni_2P acts as an electron collector for efficient separation of photogenerated carriers. Its performance is superior to that of the noble metal Pt-modified system. In 2024, Sun et al. [60] synthesized ultrathin γ-Ga_2O_3 quantum wires with a diameter of 1–2 nm by a soft template-assisted solvothermal method, utilizing strong quantum confinement effects to realize far-ultraviolet C-band photodetection. The device's spectral selectivity of R210 nm/R250 nm reaches 452, which demonstrates excellent performance.

Compared to other phases, δ-Ga_2O_3 has been relatively little studied. In 2023, Takahiro et al. [61] first experimentally confirmed the existence of δ-Ga_2O_3 and prepared δ-Ga_2O_3 thin films using the epitaxial growth technique and fog vapor deposition using β-Fe_2O_3, which has the same structure as δ-Ga_2O_3 and a small lattice mismatch as a buffer layer. The team then prepared vertical Schottky barrier photodiodes and demonstrated the semiconductor functionality of δ-Ga_2O_3. The devices were photoresponsive in the deep ultraviolet region (4.5–5.5 eV), with a photoresponsivity of 1.25 mA/W at 5.1 eV, which resolves the long-standing controversy of the existence of δ-Ga_2O_3, providing a new strategy for the stable growth of substable oxide semiconductors [62].

3. The Interface Between Ga_2O_3 and Other Materials

Metal–semiconductor contact is a crucial part of β-Ga_2O_3 power applications. For Schottky contact, the Schottky barrier height (SBH) results can be affected by the deposited metal layer and pre-metal annealing treatment process [63–68]. Ohmic contact is the key step in β-Ga_2O_3 devices. Various approaches have been proposed to improve the ohmic contact quality, such as optimizing the metal electrode, surface treatment, ion implantation, epitaxial regrowth, and adding the interlayer [69–77].

3.1. Ohmic Contact

Ohmic contacts between metals and semiconductors with low specific contact resistance and good thermal stability are necessary to realize high-performance power devices. Their specific contact resistance must be minimized to reduce voltage drop and power loss compared to semiconductor devices. Therefore, ohmic contacts with low specific contact resistance, high thermal and chemical stability, and repeatability are essential for high-performance power devices. The metal work function, metal schemes, interfacial reactions between metal and a semiconductor during the annealing process, and the doping concentration of Ga_2O_3 in the source/drain region are significant influencing factors for the ohmic contact property. Currently, almost all Ga_2O_3 devices use Ti as ohmic contacts and deposit Au as a protective layer to avoid oxidation. The ohmic contacts can be effectively formed by optimizing the metal materials, annealing conditions, source/drain doping method and concentration, and source/drain etching, as well as by adding the interlayer in the source/drain region.

For instance, in 2017, Yao et al. [78] investigated the ohmic contact properties and surface morphologies of nine metal materials, including Ti, In, Ag, Sn, W, Mo, Sc, Zn, and Zr with Sn-doped (201) β-Ga_2O_3. In 2012, Higashiwaki et al. [79] compared the I–V results of Ga_2O_3 devices with and without the RIE treatment. The RIE process was implemented by using a BCl_3/Ar mixing gas. The samples with the RIE treatment exhibited ohmic contact characteristics, while without the RIE process, the samples showed Schottky contact features. In 2024, Xin et al. [80] proposed laser annealing instead of conventional rapid thermal annealing (RTA) to investigate the ohmic contact characteristics of Ti/Au electrodes with (100) β-Ga_2O_3 substrates at different laser energy densities.

Ion implantation and epitaxial regrowth have also been reported to fabricate an ohmic contact. For instance, in 2016, Zhou et al. [70] doped β-Ga_2O_3 with Sn at a concentration of 2.7×10^{18} cm^{-3}. Combined with Ar plasma bombardment, the R_C was dramatically reduced to 0.95 Ω·mm. In order to systematically study the mechanism of heavily doped β-Ga_2O_3 using MOVPE to achieve low contact resistance, in 2022, Alema et al. [75] optimized the doping concentration, and the achieved R_C was as low as 0.023 Ω·mm.

Another approach is inserting an intermediate semiconductor layer (ISL) with a low work function and a narrower bandgap. In 2016, Oshima et al. [76] proved the insertion of indium tin oxide (ITO) for forming ohmic contact with β-Ga_2O_3.

3.2. Schottky Contact

For wide-bandgap β-Ga_2O_3, the contacts always exhibit Schottky behavior. When metal and Ga_2O_3 come into contact, the energy band of the Ga_2O_3 side bends up to make their Fermi levels equal. The lack of suitable metal materials with lower work functions makes ohmic contact formation challenging. Experimentally, the characteristic performance of the Schottky barrier is generally analyzed using I-V and C-V curves. Many research groups have investigated Schottky contacts on β-Ga_2O_3 using various metals (Ni, Pt, Au, Cu, Ir, Pd, Mo, and W) [81].

However, Jiang et al. [82] prepared SBDs of (100) β-Ga_2O_3 in contact with W, Mo, Au, and Ni and measured the SBH and the ideality factor by I-V and C-V rest. The result shows that the SBH of β-Ga_2O_3 is less dependent on the metal work functions and more influenced by the interface state, interface structure, and interactions. The Fermi level pinning effects make the surface states affect the device's performance [83]. The surface states can be reduced by oxygen plasma and annealing, chemical solution cleaning [84,85], etc.

High-temperature annealing of β-Ga_2O_3 materials prior to metal deposition can repair interfacial defects and reduce the carrier concentration. Deng [86] et al. investigated the high-temperature annealing of Ga_2O_3 in an O_2 atmosphere. Their study showed that annealing in an O_2 environment compensates the surface charge in Ga_2O_3, which increases the SBH of the metal/β-Ga_2O_3 contact and thus improves the rectification characteristics. The oxidation ambient annealing passivates the surface oxygen vacancies, resulting in a significant reduction in the reverse leakage current and a 34 nm contraction of the sizing concentration distribution to the interior, validating the surface charge compensation mechanism.

For practical applications, β-Ga_2O_3 SBDs often operate under high-temperature conditions. Thus, high-temperature performance for β-Ga_2O_3 SBDs should be investigated [67,68,87]. Also, considering that metal oxides exhibit better high-temperature stability and higher SBH, β-Ga_2O_3 SBDs utilizing metal oxides as Schottky electrodes have also been proposed and investigated [88–91]. For instance, Hou et al. [92] reported that IrOx/β-Ga_2O_3 Schottky contacts achieved a leakage current of only 2.3×10^{-9} A/cm^2 at a high temperature of 350 °C, with the rectification ratio exceeding 10^{10} at all temperatures.

Current high-temperature electronics are mainly based on Si, GaN, or SiC. However, the temperature limit for conventional silicon electronics is typically below 150–200 °C. Silicon on insulator (SOI) electronics can help reduce leakage and achieve higher performance at higher temperatures than monolithic silicon, but due to the narrower bandgap of Si (1.12 eV), the device temperature limit is still lower than 300 °C. SiC and GaN are promising materials for high-temperature applications and show particular advantages over Si for high-temperature converters, rectifiers, and microelectromechanical system (MEMS) devices. However, they are much more expensive to manufacture as compared to conventional Si electronics. Considering Ga_2O_3 has a relatively low thermal conductivity (0.11 Wcm^{-1}K^{-1}), high-temperature device properties should be studied and proposed [93,94].

In 2021, Karen et al. [95] investigated β-Ga_2O_3-based vertical Schottky barrier diodes using Pt Schottky contacts and Ti/Au ohmic contacts, constructed on (−201) oriented unintentionally doped n-type substrates. Temperature-dependent electrical tests revealed a Schottky barrier height of about 1.2 eV and a Richardson constant of 20 A/cm^2·K^2. The device turn-on voltage dropped to 0.1 V at 400 °C. The switching ratio decreased from room temperature > 10^9 to 17. After 10 thermal cycles at 400 °C, the series resistance at room temperature increased by a factor of 1000 (from 0.1 Ω·cm^2 to 24 Ω·cm^2), mainly originating from the Ti ohmic contact layer migrating to the surface through the Au electrode and oxidizing. STEM-EDS characterization confirms that Ti diffuses and oxidizes at elevated temperatures, leading to contact degradation. The results indicate that the high-temperature reliability of Ga_2O_3 diodes is limited by the stability of the ohmic contacts. The contact structure needs to be optimized to break through the 400 °C application limit. This study clarifies the contact reliability bottleneck for high-temperature applications of Ga_2O_3 devices, which provides an experimental basis for designing high-temperature-stable

Ga_2O_3 power/sensor devices, and promotes their applications in extreme environments such as aerospace and nuclear energy.

Also, in 2021, Hou et al. [96] investigated the improved rectification performance of Pd Schottky contacts (SCs) on β-Ga_2O_3 at high temperatures. Experiments on Pd SCs on the (−201) and (010) crystal planes of β-Ga_2O_3 exhibit a significant improvement in the rectification performance when operated at high temperatures in air. The image-force-corrected barrier heights ($\Phi_{B,IF}$) increased from 1.40 eV at room temperature to 1.75–2.20 eV at 500 °C, with the main transition occurring at 250–450 °C. This is attributed to the oxidation of the Pd layer to form high-barrier PdO regions dominating the high-temperature current transport. The optimized oxidized Pd SCs have a $\Phi_{B,IF}$ of 2.20 eV at 500 °C, a leakage current of ~1×10^{-6} A/cm^2 (−3 V), and a rectification ratio (±3 V) of ~10^7, which is comparable in performance to the best results of diamond and SiC. In addition, the temperature dependence of the built-in voltage of thermally oxidized Pd SCs is highly compatible with the β-Ga_2O_3 optical bandgap (both −1.3 meV/°C) in the room temperature to 500 °C interval. This study provides a key solution for β-Ga_2O_3 high-temperature device applications.

In 2023, Shahadat et al. [97] investigated the optimized p-NiO/n-β-Ga_2O_3 heterojunction diodes, grown with a NiO layer by pulsed laser deposition (PLD) and processed by bench etching and annealing. The rectification ratio is over 10^6 at 410 °C, the turn-on voltage is about 0.8 V, and the reverse leakage current is below the lower limit of the measured noise, which is better than that of Ni-based Schottky diodes. Mott–Schottky analysis and TCAD modeling confirm that a higher built-in potential (~1.9 V) and additional band shift are key to performance improvement, providing solutions for high-temperature sensors and power electronics. In addition, further efforts should be taken with respect to optimizing the quality of the interface traps and the NiO layer for further improvement.

The high-temperature operation of β-Ga_2O_3 SBDs significantly affects the critical characteristics of the devices, such as the Schottky barrier height, ideal factor, leakage current, on-state voltage, and breakdown voltage, which reduces the performance and reliability of the devices. In 2025, Nahid et al. [98] used in situ transmission electron microscopy (TEM) for the β-Ga_2O_3 SBD to observe the defect nucleation and evolution process in real time under forward bias and high-temperature conditions. Their study reveals the failure mechanism of the formation of vacancy clusters and amorphous regions due to high-temperature electrothermal stresses, as well as the formation of metal pools by metal diffusion from Ni/Au electrodes, which ultimately triggers the breakdown of the device and provides key insights for improving the high-temperature reliability of β-Ga_2O_3 devices.

In 2025, Wang et al. [99] investigated the properties of β-Ga_2O_3/AlN heterojunctions at high temperatures. The heterojunction was grown by MOCVD, and XPS analysis confirmed a type II energy band arrangement, which is favorable for electron accumulation. The β-Ga_2O_3 thermal conductivity of 4.2 W/(m·K) and the interfacial thermal conductivity of 118.6 MW/(m^2·K) were measured by the TDTR method, which showed an excellent heat dissipation capability. The prepared SBDs exhibited low turn-on voltage (0.1 V), ideal factor of 4.22, modified Richardson's constant of 48.5 A/cm^2K^2, and high breakdown voltage of 1260 V at high temperature at 300–420 K, which proved their good potential for application in high-temperature environments.

Despite the advantages of low cost and high performance for β-Ga_2O_3, it is still challenging to achieve p-type β-Ga_2O_3. Thus, this research is mainly focused on unipolar power devices, such as Schottky barrier diode (SBD) and MOSFET [100–109]. In addition, its wide-bandgap property enables it as a crucial material for the next generation of deep-ultraviolet light (DUV) photodetectors [43,110–113]. For power applications, by improving the quality of the epitaxial layer and optimizing the device structure and fabrication process, the β-Ga_2O_3 SBDs have been developing in the direction of higher V_{BR} and lower $R_{ON,SP}$, along with the MOSFET devices. For instance, in 2025, Chang et al. [114] proposed a vertical β-Ga_2O_3 SBD with junction termination extension (JTE) utilizing a sputtering p-GaN layer; the SBD achieves a V_{BR} of 3 kV with a low $R_{ON,SP}$ of 6.15 mΩ·cm^2 and high Baliga's figure of merit of 1.46 GW/cm^2. For β-Ga_2O_3 MOSFET, Wang et al. [115] fabricated a reduced surface electric field (RESURF) p-NiO_X/n-β-Ga_2O_3 heterojunction FET (HJ-FET) with optimized t_{NiO} = 110 nm. The devices exhibited a high V_{BR} of more than 10 kV and PFOM of 63 MW/cm^2.

4. Approaches to β-Ga_2O_3 Power Diodes

Diodes are key components in integrated circuits (ICs), which can act as rectification, signal modulation, etc. [116–119]. β-Ga_2O_3 power diodes have become a current research topic in the field of power electronics due to their excellent electrical properties and power application potential. In order to improve the device performance, researchers have proposed many new device structures, including SBDs and pn junction diodes with lateral and vertical structures using different techniques. Some other representative diodes have also been proposed in recent years and will be discussed in sequence.

4.1. Schottky Barrier Diode (SBD)

Due to the absence of the minority carrier storage effect, SBDs are promising to obtain a low switching loss and fast switching speed. In addition, SBDs typically have a lower on-state voltage (V_{ON}) thanks to the low barrier height. In recent years, researchers have devoted significant efforts to improve the V_{BR} and overall device performance of the proposed SBDs, owing to their simple fabrication process. In 2013, Sasaku et al. [120] proposed the early β-Ga_2O_3 SBD fabricated on single-crystal substrates without passivation or edge termination, as shown in Figure 1a. The fabricated SBD exhibits good rectification characteristics. The V_{BR} and $R_{ON,SP}$ of the fabricated SBD are 150 V and 3 mΩ·cm^2, respectively. The calculated Schottky barrier height is 1.3–1.5 eV. However, compared to the bipolar devices, the SBD exhibits inferior breakdown characteristics since the unidirectional transport of carriers is determined by the Schottky barrier formed by the metal/semiconductor contact.

To improve the V_{BR}, the power SBD structure incorporates a lightly doped drift layer. In 2015, Higashiwaki et al. [121] fabricated Ga_2O_3 SBDs with a 7 μm thick Si-doped n-type drift layer, as shown in Figure 1b. The V_{BR} of the fabricated SBDs is enhanced to 150V, with a low $R_{ON,SP}$ of 2.4 mΩ·cm^2. In addition, in 2016, as shown in Figure 1c, Oda et al. [122] proposed an n^- Ga_2O_3/n^+ Ga_2O_3 structure SBD. By optimizing the thickness of n-Ga_2O_3 layer, the $R_{ON,SP}$ can be reduced as low as 0.1 mΩ·cm^2. The optimized V_{BR} reaches around 855V. Other factors also affect the electrical characteristics, including electrode size, device area, crystallographic planes, and surface treatment [123–131]. For instance, in 2021, He et al. [126] removed the donor-like impurities at the top of the drift region by inductively coupled plasma (ICP) etching, which effectively suppressed the surface recontamination and the leakage current of the β-Ga_2O_3 SBDs, resulting in a high V_{BR} of 1720 V and an outstanding PFOM of 1.32 GW/cm^2. In 2025, Deng et al. [86] also used ICP etching to improve the surface quality of β-Ga_2O_3 thin films. By optimizing the BCl_3/Ar ratio to 35/5, the V_{BR} reaches 1500 V with a corresponding $R_{ON,SP}$ of 4 mΩ·cm^2. The underlying mechanism is also discussed. Also, Lee et al. [129] proposed the first wet surface treatment of tetramethylammonium hydroxide (TMAH) on β-Ga_2O_3 surfaces and demonstrated the effectiveness of TMAH treatment in enhancing the performance of β-Ga_2O_3-based devices. In 2025, Yu et al. [130] presented a low-temperature post-annealing (LTPA) technique to improve the forward performance and V_{BR} of β-Ga_2O_3 SBDs, realizing a low ideality factor of 1.00 and subthreshold swing of 60–61 mV/decade. The V_{BR} of SBDs treated with LTPA at 350 °C increases by 48%. Moreover, in 2025, to reduce the cost, Liu et al. [131] used a thermal oxidation (TO) technique to prepare vertical Ga_2O_3 SBDs directly on heavily doped single-crystal (001) β-Ga_2O_3 substrates without epitaxial growth, as shown in Figure 1d. By optimizing the annealing temperature and time (900 °C, 2 h), the β-Ga_2O_3 SBDs achieve a V_{BR} of 460 V, $R_{ON,SP}$ of 10.5 mΩ·cm^2, and PFOM of 20.2 MW/cm^2. This technique provides a new method to reduce the cost of such devices.

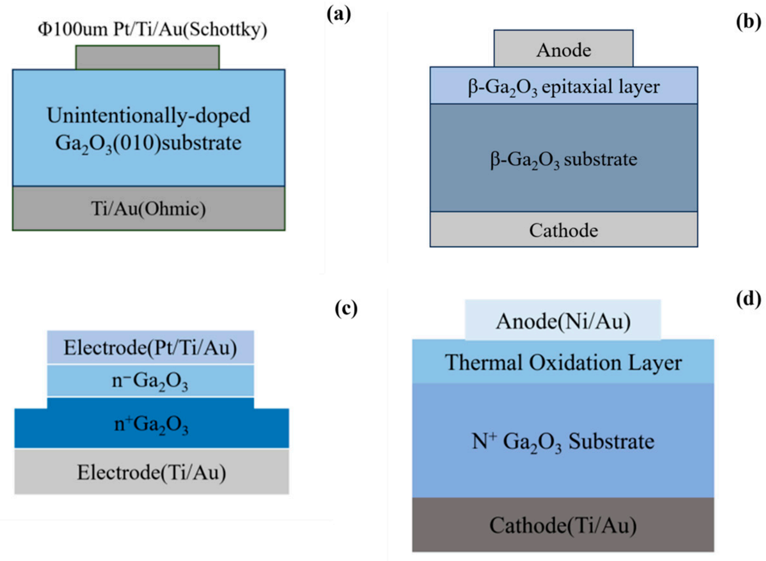

Figure 1. (**a**) Cross-sectional schematic illustration of the proposed Ga_2O_3 SBDs [120], (**b**) Ga_2O_3 SBDs with Si-doped n-type drift layer [121], (**c**) n^--Ga_2O_3/n^+-Ga_2O_3 structure SBD [122], and (**d**) TO-SBD [131].

4.1.1. Field Plate (FP) Technique

As shown in Figure 2, the breakdown of vertical β-Ga_2O_3 SBDs usually originates from the high electric field intensity at the edges of the Schottky metal electrodes. The field plate (FP) technique, by introducing additional metal electrodes at the edges of the device, can redistribute the electric field to reduce the localized electric field intensity. For this reason, the V_{BR} can be enhanced, and the structure is widely used in SiC and GaN power devices [132–135]. For β-Ga_2O_3 SBDs, in 2017, Konishi et al. [136] reported the early FP technique with SiO_2 as support material. The achieved V_{BR} exceeds 1 kV (1076 V), with a low $R_{ON,SP}$ of 5.1 mΩ·cm^2. By replacing the SiN_X as the FP oxide material, in 2018, Yang et al. [123] fabricated the β-Ga_2O_3 SBDs with the high V_{BR} of 2.3 kV, with circular diode diameters of 150 µm, as shown in Figure 3b. The cross-sectional view of the device can be seen in Figure 3a. Also, high-k dielectric can be selected as the FP oxide material. In 2025, Wang et al. replaced the dielectric layer material with high-k HfO_2 and found that the thickness of the dielectric layer has a certain effect on the peak electric field of the device. The thicker the thickness of the dielectric layer is, the weaker the voltage-sharing ability of the field plate is. When the thickness of the dielectric layer T_{ox} = 170 nm, the FP has the best effect on the improvement of V_{BR}, which raises the V_{BR} from 543 V to 760 V. At an earlier time, Roy et al. [137] used the high-k $BaTiO_3$ (BTO) and $BaTiO_3$/$SrTiO_3$ (BTO/STO) as oxide FP material, and the V_{BR} of the fabricated SBD increased from 148 V (without FP) to 486 and 687 V, respectively. Also, by using BTO as the field plate dielectric on a β-Ga_2O_3 wafer with the epitaxial layer thickness of 11 µm, the devices obtain a V_{BR} of 2.1 kV, 2.7 times higher than that of SBD without field plates [138]. Other high-k materials can be used as FP oxide, such as TiO_2, Al_2O_3, and PtO_x [139–141].

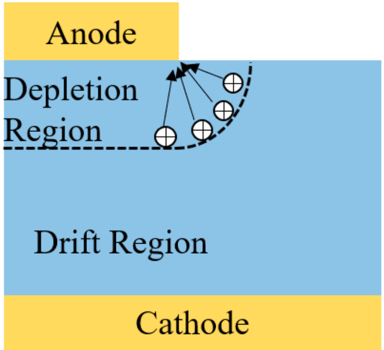

Figure 2. Concentration of the electric field distribution of the Ga_2O_3 SBDs.

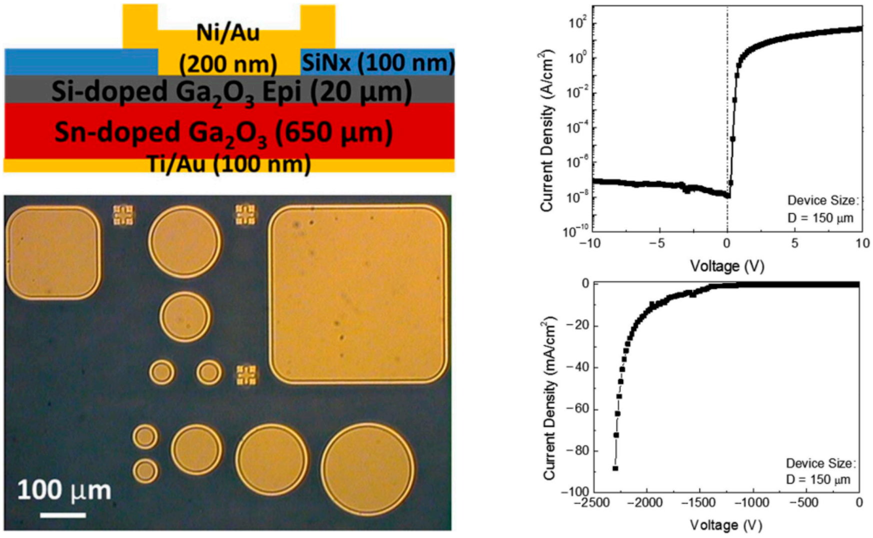

(**a**) (**b**)

Figure 3. (**a**) Schematic of edge-terminated, vertical geometry Ni/Au Schottky rectifier structure (**top**) and top-view optical microscope image of the device layouts (**bottom**) showing different device areas; (**b**) expanded view of forward (**top**) and reverse (**bottom**) J-V characteristics for the 150 µm diameter rectifier [123].

Instead of a single field plate, bilayer field plate and three-step field plate techniques have also been proposed for improving the SBD electrical performance. In 2019, Yang et al. [142] deposited a SiO_2/SiN_x double-layer dielectric as a field plate by using PECVD, and the schematic can be seen in Figure 4a. The composite SiO_2/SiN_x FP oxide is used in this work to suppress the electric field crowding. The Schottky electrode diameter is 1mm, the current can reach 1 A when the voltage is set to 2.3 V, and the V_{BR} reaches 760 V. In 2024, Yuda et al. [143] demonstrated that a dual FP-SBD design improves the V_{BR} through experimental and TCAD simulation methods, and the V_{BR} reaches 2082 V with an $R_{ON,SP}$ of 6.9 mΩ·cm^2 at drift layer thicknesses of 135 nm and 425 nm for FP1-SiO_2 and FP2-SiO_2, respectively, which helps to achieve a balance of high breakdown voltage and low on-resistance to drive β-Ga_2O_3 in the field of power devices. In 2025, Lee et al. [144] proposed a vertical Au/Ni/β-Ga_2O_3 Schottky barrier diode with a regularly arranged internal field plate with the structure shown in Figure 4b. The results show that the SBD with regularly arranged inner field plates exhibits an improved V_{BR} of 590 V as compared to the regular one. Simulation using a TCAD technique shows that the regularly arranged inner field plates can effectively suppress the peak electric field distribution under the anode edge, thus improving the V_{BR}. In addition, in 2024, Gilankar et al. [145] proposed vertical Ga_2O_3 SBD integrated with a combination of three field plates and nitrogen ion implant for field termination. The schematic of the proposed SBD can be seen in Figure 4c. The optimized diodes exhibit a low $R_{ON,SP}$ of 6.2 mΩ·cm^2 and a high breakdown voltage of about 1400 V, with a reverse leakage current lower than 10^{-4} A·cm^{-2} up to a voltage of 1.25 kV. Other representative related investigations have also been proposed and reported [146–148].

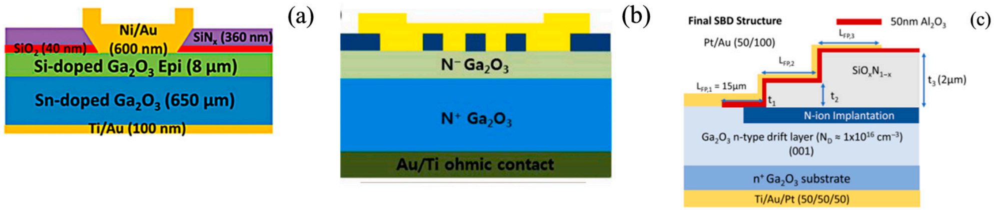

Figure 4. (**a**) device schematic of vertical β-Ga_2O_3 SBDs with a bilayer field plate [142]; (**b**) vertical Au/Ni/β-Ga_2O_3 Schottky diodes with regularly aligned inner field plates [144]; (**c**) the final fabricated SBD structure with different dielectrics and metal contacts [145].

Moreover, the FP angle plate plays an important role in improving the electric field distribution. In 2019, Allen et al. [149] fabricated a small-angle beveled mesa and field plate structure with an angle of 1°. The schematic of the proposed small-angle beveled field plate (SABFP) β-Ga_2O_3 SBDs is illustrated in Figure 5a. In their work, SBDs with simple structures, ordinary field plate structures, and 45° beveled field plate (BFP) structures are also fabricated for comparison. As shown in Figure 5b, the corresponding V_{BR} values are ~200 V, ~400 V, ~650 V, and ~1100 V, respectively. The results demonstrate that SABFP is effective in suppressing the peak E-field at the Schottky edge in both SOG and Ga_2O_3, resulting in high V_{BR}. In 2021, Liu et al. [150] investigated the influence of the dielectric bevel angle, field plate length, and dielectric materials on the V_{BR} of the proposed SBD by TCAD study. The results proved that the edge termination structure of the small-angle beveled field plate can alleviate the electric field concentration effect and improve the breakdown voltage. In 2022, by using a field plate-assisted negative beveled (FP-NB) terminal, Chen et al. [151] fabricated the SBD with a V_{BR} of 1100 V and $R_{ON,SP}$ of 2.6 mΩ·cm$^{2.}$ Also, the electric field distribution of bevel terminations with mesa angles has been studied using TCAD. Other results of FP-SBDs have also been presented by researchers [152–155].

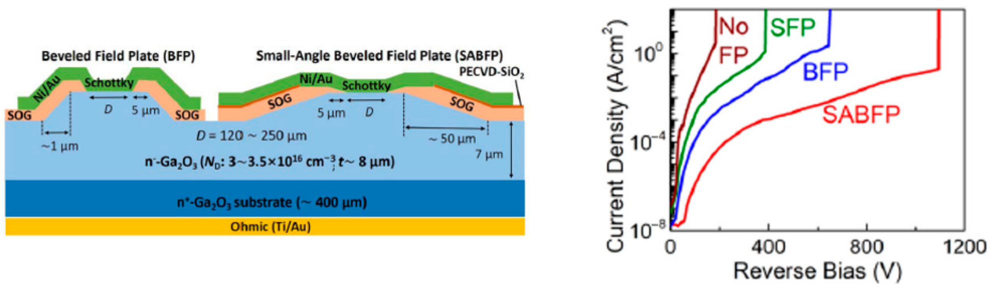

(**a**) (**b**)

Figure 5. (**a**) Schematics of vertical Ga_2O_3 SBDs with (**a**) BFPs and SABFPs; (**b**) reverse I-V characteristics of the SBDs with no FPs, SFPs, BFPs, and SABFPs [149].

In conclusion, the field plate technology has become the core solution for β-Ga_2O_3 SBDs to improve the voltage withstand capability by virtue of the process compatibility and significant electric field modulation effect. In the future, it is necessary to further optimize the dielectric layer materials and the metal deposition process for further improving the β-Ga_2O_3 SBD performances.

4.1.2. Edge Terminal (ET) Technique

Besides the FP technique, the formation of a high resistivity region at the edge of the anode can promote the potential diffusion along the surface and suppress the peak electric field, which can effectively suppress the reverse leakage current while improving the V_{BR}. This technique is a more complex process, while reducing the geometric discontinuities. There are two main methods to form a high-resistivity region in β-Ga_2O_3: ion implantation and oxygen annealing. Ion implantation is the most commonly used method due to the fact that it is easier to choose the injection region. The injected ions can act as deep bodies to introduce deep energy levels to compensate for carriers, and the lattice damage caused by ion bombardment can introduce energy levels in the middle of the band gap to trap carriers. This results in a lower electron concentration and higher resistance in the ion injection region. A number of ion implantation terminals have been shown to improve the breakdown voltage, including N, Ar, F, He, Mg ions, etc. For instance, in 2019, as shown in Figure 6a, Zhou [156] prepared vertical β-Ga_2O_3 SBDs using Mg ion implantation for edge terminals (ETs). In their results, as shown in Figure 6b, the reverse V_{BR} of vertical Ga_2O_3 SBD with ET at a R = 90 µm achieves 1.55 kV, significantly higher than that (500 V) of the one without ET. Combined with the $R_{ON,SP}$ of 5.1 mΩ·cm^2, the PFOM is calculated to be 0.47 GW/cm^2. In their latter work, Zhang et al. [157] found that He and Mg ion implantation were able to increase the V_{BR} of the device from 0.5 kV to 1.0 kV and 1.5 kV, respectively. The SBDs with Mg ion implantation exhibit higher V_{BR} than He, but traps or defects in the ion implantation region lead to the degradation of forward and off-state stresses, which can severely affect the device's reliability and dynamic performance.

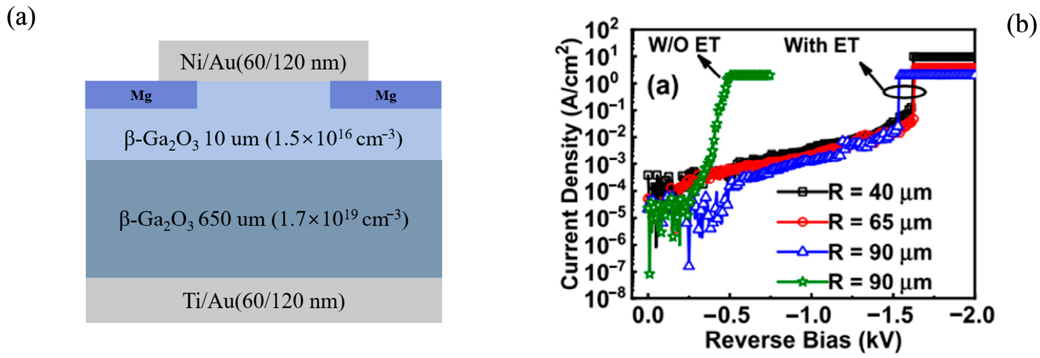

Figure 6. (**a**) Cross-section schematic view of the vertical β-Ga_2O_3 SBD with Mg implanted ET; (**b**) semi-log plot of the reverse I–V characteristics of the vertical β-Ga_2O_3 diode with and W/O Mg-implanted ET [156].

In addition, for the Ar ion implantation technique, Gao et al. [158] prepared vertical β-Ga_2O_3 SBDs using Ar ion implantation for edge terminals, with the injection energy of 50 keV and doses of 5×10^{14} cm^{-2} and 1×10^{16} cm^{-2}. The V_{BR} was enhanced from 209 V to 252 V and 451 V. The PFOM also increased from 25.7 to 30.2 and 61.6 MW/cm^2, an increase of 17.5% and 140%, respectively. In 2020, Hu et al. [159] proposed a novel vertical β-Ga_2O_3 SBD based on a self-aligned beveled fluorine plasma treatment (BFPT) edge termination structure. Thanks to the strong electronegativity of fluorine ions, the fixed negative charges introduced by F ions can alleviate the electric field crowding around the junction periphery, resulting in the high V_{BR} of 1050 with a relatively low $R_{ON,SP}$ of 2.5 mΩ·cm^2. Later in 2024, Luo et al. [160] proposed the F-ion injection into SiN_x trench termination structure, where F ions are injected into SiN_x at a shallower injection depth than into β-Ga_2O_3, which effectively mitigates the lattice damage of β-Ga_2O_3 by ion injection, reduces the required injection energy, and improves the reliability of the device. When the injection depth is 600 nm, the F-injection dose is 3.3×10^{13} cm^{-2}, and the maximum V_{BR}

of the device is 4734 V, with the low $R_{ON,SP}$ of 2.1 m$\Omega\cdot$cm^2. For this reason, the obtained PFOM is as high as 10.7 GW/cm^2. In 2019, Lin et al. [161] proposed the guard ring (GR) technique formed by N ion implantation, aiming to improve the V_{BR}. For comparison, four types of SBD structures with (1) neither a GR nor a FP, (2) a GR, (3) a FP, and (4) both a GR and a FP were fabricated on the same substrate. From their results, the GR/FP SBD exhibits the highest V_{BR} of 1430 V, with the low $R_{ON,SP}$ of 4.7 m$\Omega\cdot$cm^2. In 2025, Feng et al. [106] studied the performance of a large-size (3 $\times$ 3 mm^2) vertical β-Ga_2O_3 SBD using a dual-field plate and N-ion implantation edge termination structure. V_{BR} of 1.5 kV, $R_{ON,SP}$ of 9.2 m$\Omega\cdot$cm^2, forward current (IF) of 11.2 A, peak inrush current of 58 A, and a reverse recovery time and losses comparable to those of a commercial 30 A SiC diode at a voltage of 2 V were achieved. The device outperforms other similar devices and has great potential for commercial applications. Other outstanding related works using ion implantation at the edge terminal [162–165] have also been proposed and studied.

Unlike GaN and SiC, annealing in an oxygen atmosphere promotes the compensation of gallium vacancies, thereby reducing the carrier concentration of β-Ga_2O_3. This makes oxygen annealing a unique method for the formation of high resistivity (HR) regions in β-Ga_2O_3. As shown in Figure 7a, Wang et al. [166] deposited a layer of SiO_2 as a barrier layer to select the HR region and investigated the difference in device performance after annealing at different temperatures. The V_{BR} of the devices annealed at 400 °C increased significantly, while the $R_{ON,SP}$ increased slightly, which can be seen in Figure 7b. However, the $R_{ON,SP}$ increases rapidly with annealing temperature beyond 600 °C. The suspected reason is that higher annealing temperatures (>600 °C) result in sharp degradation of the ohmic contacts and the limited blocking ability of SiO_2 at high temperatures. A more effective barrier layer under high annealing temperatures is needed to fully utilize the oxygen annealing technique. To address these issues, He et al. [167] used polysilicon as an annealing cover layer to realize a selective high barrier zone for β-Ga_2O_3 wafers at 1100 °C. Experiments showed that there was no significant loss of carrier concentration in the polysilicon zone (~1.8 $\times$ 10^{16} cm^{-3}), while the exposed zone showed significant loss of carrier concentration (3.0 $\times$ 10^{14} cm^{-3}), with a depletion depth of 2.4 μm, demonstrating the desirable blocking ability of polysilicon for oxygen annealing environments. The device with L_{ET} = 15 μm has an $R_{ON,SP}$ of 4.1 m$\Omega\cdot$cm^2, a V_{BR} of 1800 V, and a PFOM of up to 0.78 GW/cm^2, demonstrating the advantages of the thermal oxidation method. Details of the mechanism of the thermal oxidation method can be seen in Refs. [84,168–171]. In addition, Dong et al. [172] fabricated the β-Ga_2O_3 SBDs with the SiO_2 lying under the anode edge to support the high peak electric field. The high V_{BR} of 5–6 kV and low $R_{ON,SP}$ of 3.4 m$\Omega\cdot$cm^2 are achieved simultaneously in their results, leading to the excellent PFOM to be 7.4–10.6 GW$\cdot$cm^{-2}.

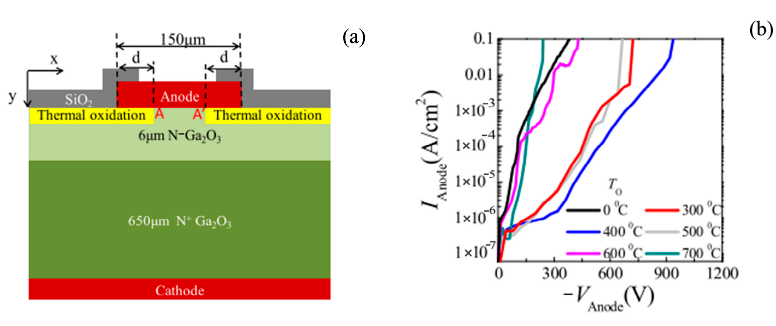

Figure 7. (**a**) Schematic cross-section of β-Ga_2O_3 SBD with thermally oxidized termination. (**b**) Reverse I–V characteristics of unterminated SBD and OT-SBD with different thermal temperatures [166].

This technique effectively modulates the electric field distribution of β-Ga_2O_3 devices through ion implantation or oxygen annealing, significantly enhancing the V_{BR} and suppressing the reverse leakage current. However, the potential of the ion-implanted and thermally oxidized end-junction structures needs to be further explored experimentally, and future research could focus on ion-implanted damage repair and oxygen annealing depth modulation to further promote the commercialization of β-Ga_2O_3 power diodes.

4.1.3. Trench MOS Technique

Trench MOS SBD is a novel device structure based on conventional SBDs, introducing a trench structure combined with the MOS (metal-oxide-semiconductor) principle. The core feature is a vertical trench etched on the semiconductor surface, which transforms the planar Schottky junction into a three-dimensional trench junction and forms the oxide layer and gate electrodes of the MOS structure on the sidewalls of the trench. This design combines the advantage of a low forward voltage drop of SBD with the electric field modulation capability of the MOS structure, showing unique advantages in ultra-wideband semiconductors such as β-Ga_2O_3. In 2017, Sasaki et al. [173] prepared β-Ga_2O_3 trench MOS SBDs for the first time on β-Ga_2O_3 substrates with a 7 μm drift layer (6×10^{16} cm^{-3}), as illustrated in Figure 8a. The experiments demonstrated that the trench MOS SBDs are effective in reducing the reverse leakage current, increasing the V_{BR} from 70 V to 240 V. Due to the reduced current channel, the $R_{ON,SP}$ increased from 2.3 mΩ·cm^2 to 2.9 mΩ·cm^2. For trench MOS SBDs, the dimensions and fabrication process may affect the SBD performance and have been studied.

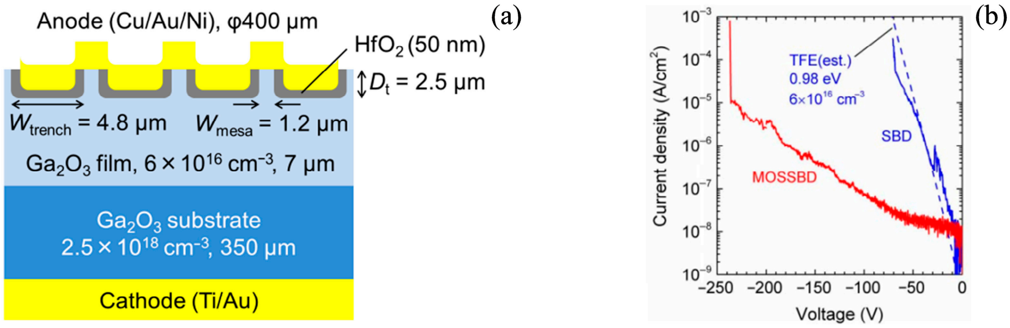

Figure 8. (**a**) Schematic cross-section of β-Ga_2O_3 trench MOS SBD. (**b**) Reverse I-V characteristics of β-Ga_2O_3 trench MOS SBD [173].

In 2018, Li et al. [174] proposed β-Ga_2O_3 trench MOS SBDs on β-Ga_2O_3 substrates with a 10 μm drift layer (1–2×10^{15} cm^{-3}), realizing a V_{BR} of 1.5 kV, with a reduction of four orders of magnitude in the reverse leakage current with respect to conventional SBDs. In the same year, they further experimented on a substrate with a drift layer concentration of 2×10^{16} cm^{-3} and obtained a similar device with a V_{BR} of 1232 V, which demonstrated that increasing the epitaxial layer doping concentration can lead to a reduced V_{BR}. They also proved that decreasing the fin width enhances the surface electric field effect, which results in lower leakage current and improved V_{BR} [175]. In their later work [176], they minimized the etch damage by introducing wet etching to achieve rounded trench corner profiles to reduce the electric field crowding, featuring a V_{BR} of 2.44 kV and a PFOM of 0.39 GW/cm^2. In 2020, Huang et al. [177] optimized the trench corner radius and the length of the trench by TCAD simulation. They found that optimizing the trench corner radius could reduce the maximum field strength of the dielectric layer and increase the breakdown voltage. Finally, they proposed the Ga_2O_3 trench SBDs with a high V_{BR} of 3.4 kV and a PFOM of more than 1.7 GW/cm^2. In the same year, Li et al. [178] optimized the fin width by means of a field plate to optimize the device structure, as shown in Figure 9a; they found that the field crowding at the trench corners is caused by the positive space charge inside the fin channel. By reducing the fin channel width, the total space charge inside the fin channel was reduced, thus reducing the field crowding at the trench corners. The V_{BR} reached 2.89 kV with the field plate, as shown in Figure 9b, which is about 500 V higher than that without the field plate, and the coefficient of Baliga was 0.95 GW/cm^2. Subsequently, in 2025, Yi et al. [179] proposed β-Ga_2O_3 trench Schottky barrier diodes with double-field plate termination and an Al_2O_3/SiN dielectric layer structure, where the dual-field plate consists of Al_2O_3/SiN/Ni (the first FP) and Al_2O_3/SiN/Ti/Al (the second FP). The second FP helps to reduce the electric field crowding effect at the edges of the first FP, thereby increasing the V_{BR} of the thin double-layer dielectric (Al_2O_3/SiN) at the edges of the first FP. The V_{BR} of the proposed SBDs is increased from 700 V in conventional SBDs to 1380 V with an $R_{ON,SP}$ of 6.06 mΩ·cm^2. The PFOM is improved from 31 MW/cm^2 to 314 MW/cm^2. In 2024, Kim et al. [180] systematically investigated the instability of turn-on voltage for β-Ga_2O_3 trench SBDs with different finned channel orientations under a forward bias of 3~10 V. Among them, fins oriented along the [010] direction exhibit the highest turn-on voltage stability and the smallest hysteresis, whereas finned channels oriented along the [100] direction exhibit the largest instability. This study reveals the correlation between the charge trap effect and the fin channel orientation, which provides ideas for the optimized design of the β-Ga_2O_3 SBD. In 2025, Dhara et al. [181] proposed a method to realize charge recovery after ICP-RIE etching by ultra-high vacuum annealing and prepared the multi-fin channel SBDs. SBDs with [100] and [010] orientations exhibit comparable on-resistance. The V_{BR} of the proposed multi-fin trench SBD is up to 1.85 kV, and the through-breakdown electric field is over 3.2 MV/cm. This study solves the problems of charge compensation and on-resistance increasing during the etching process, improving the device's efficiency and performance. In order to mitigate the effect of the trench structure on the forward conduction current, Ji et al. [182] proposed the edge trench field-limited ring (TFLR) structure by introducing an edge trench structure near the Schottky metal. The results show that the TFLR structure significantly increases the V_{BR}, reducing the reverse leakage current of the device while maintaining good forward conduction characteristics. The TFLR structure enhances the V_{BR} of the device from 190 V to 1010 V, and the reverse leakage current reduces from 3.16×10^{-8} A/cm^2 to 6.21×10^{-10} A/cm^2. Other representative and related work using trench MOS SBDs has also been studied and proposed [183–189].

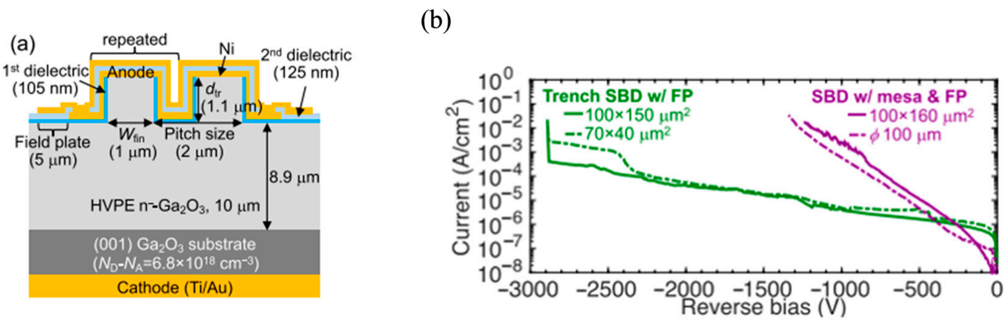

Figure 9. (**a**) Schematic cross-section of the field-plated Ga_2O_3 trench SBDs. (**b**) Comparison of the reverse I-V characteristics between field-plated trench SBDs and SBDs with mesa [178].

In summary, the trench MOS structure has significantly improved the V_{BR} and suppressed the leakage current of β-Ga_2O_3 power diodes through electric field modulation and interface engineering, and in particular, the combination of high-k dielectrics and field plate technology has pushed the V_{BR} to exceed 3000 V. In the future, efforts should be focused on the repair of etch damages, compatibility of the dielectric layer, and large-area homogeneity in order to accelerate the commercialization of the structure for ultra-high-voltage β-Ga_2O_3 power devices.

4.1.4. Mesa Termination Technique

The mesa termination technique is another useful method, realized by an etching process that increases the Schottky contact area to reduce the electric field concentration at the edge of the electrodes and improve the device's electrical performance. In 2022, Dhara et al. [190] proposed a deep bench etching design for β-Ga_2O_3 SBDs to achieve efficient fringe electric field termination, with the structure shown in Figure 10a. The V_{BR} was increased from 350 V to 1150 V at an etch bench depth of 4 μm. They also analyzed the effect of dry etching based on BCl_3/Cl_2 on (100) and (010) sidewalls and observed depletion anisotropy of the etch along different sidewalls. Simulations and experiments show that deep etching significantly improves the electric field termination efficiency and V_{BR} with little effect on the device conduction characteristics. Also, Han et al. [191] proposed a novel Ga_2O_3 SBD combined with platinum oxide (PtO_x) and anodic self-aligned stage termination (SAMT), as shown in Figure 10b. They systematically investigated the effect of different stage etching depths on the performance of the devices. Their results showed that the V_{BR} reaches 2738 V at an etching depth of 1.2 μm, 2.44 times higher than that of the unetched device. In addition, the leakage current density of the device at −2000 V is lower than 10 μA/cm^2, which provides an effective method to improve the V_{BR} and reduce the leakage current of β-Ga_2O_3 SBDs. This method combines PtO_x anodes to increase the barrier height while maintaining lower leakage current, but a higher barrier height inevitably leads to higher on-state voltage, which increases the on-state loss of the device.

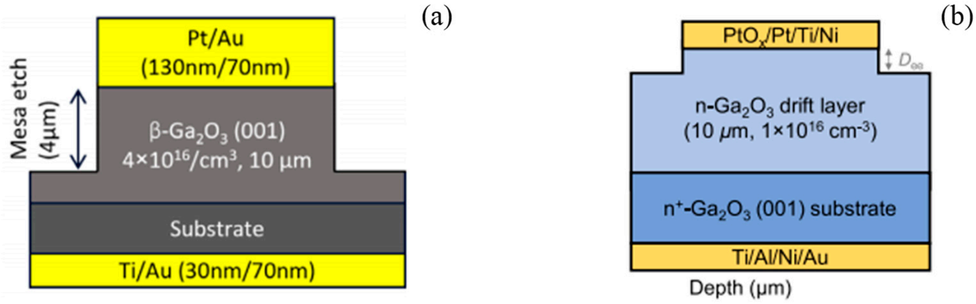

Figure 10. (**a**) Schematic cross-section of the mesa-etched β-Ga_2O_3 Schottky barrier diodes [190]. (**b**) β-Ga_2O_3 SBD with SAMT [191].

Some factors affect the electrical characteristics, including the inclination angle of the mesa, etching, or treatment method. In 2025, Zhang et al. [192] proposed a β-Ga_2O_3 trench MOS barrier Schottky (TMBS) diode with a novel termination structure of positively beveled countertop and curved bottom corners, which were fabricated with O_2 plasma, hydrofluoric acid (HF), and tetramethylammonium hydroxide (TMAH) post-etching treatment. The effects of the three treatment techniques on the electrical characteristics of the devices were investigated. It was found that the on-resistance of the three treatments was similar at about 2.6 mΩ·cm^2 and that V_{BR} values were 1280 V, 1440 V, and 1800 V, respectively. The post-etching technique improves the V_{BR} by optimizing the β-Ga_2O_3 etched surface. TMAH reduces the surface roughness, and O_2 plasma reduces the oxygen vacancies, and a combination of both may be a better repair method. At an earlier time, Chen et al. [151] proposed β-Ga_2O_3 SBDs with negative- and positive-beveled mesa structures, respectively. Compared to regular SBDs, the V_{BR} of the negative-beveled (NB) mesa structure was increased from 400 V to 1100 V. While for the positive-beveled (PB) mesa structure, a high V_{BR} of 1710 V is achieved due to the more mitigated electric field concentration.

Field plates can likewise be combined with mesa termination structures to improve the device performance. In 2024, Wan [193] proposed β-Ga_2O_3 SBDs with a field plate-assisted deep mesa (FPDM) termination structure, which effectively reduces the anode edge electric field by forming a deep table through self-aligned etching and incorporating a field plate, as shown in Figure 11. In their work, experimental results show that the fabricated FPDM-SBD has a V_{BR} of over 2.5 kV, an $R_{ON,SP}$ of 3.78 mΩ·cm^2, a power quality factor of 1.65 GW/cm^2, and a forward voltage as low as 1.45 V, demonstrating the potential of the β-Ga_2O_3 SBD for multi-kilovolt applications. In addition, Feng et al. [194] proposed SBDs with a composite termination structure of mesa and double-field plates combined with a substrate thinning process. This composite termination results in an increase in V_{BR} from 400 V to 1240 V, with substrate thickness thinning to 85 μm, reduction in on-resistance from 174 mΩ·cm^2 to 112 mΩ·cm^2, an increase in forward current from 6.04 A to 10.1 A, and an increase in inrush current from 20 A to 29 A. Thermal resistance is significantly reduced from 6.45 K/W to 2.21 K/W, comparable to commercial SiC SBDs.

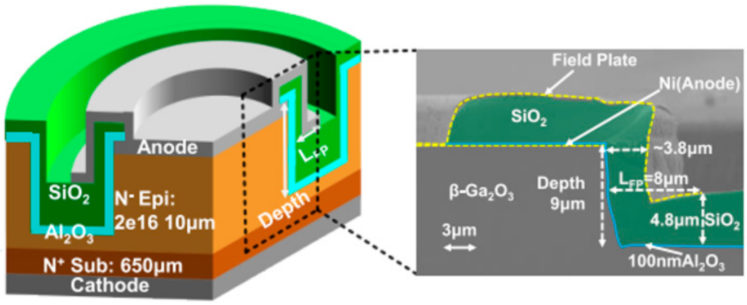

Figure 11. Schematic cross-section of the fabricated FPDM-SBD and its SEM image [193].

Sun et al. [153] proposed a hybrid electric field management configuration combining a beveled mesa (BM) termination with a high-k oxide $BaTiO_3$ field plate (FP), which can effectively suppress the electric field crowding at the edge of the anode and increase the V_{BR} to 1726 V, which is superior to the BM-terminated SBD with a V_{BR} of 0.64 kV and the bare SBD with a V_{BR} of 0.22 kV. The BMFP-SBD exhibited excellent dynamic switching characteristics, with a short reverse recovery time of 10.1 ns, and is virtually unaffected by high-k dielectrics even under switching conditions, with di/dt as high as 420 A/ls, realizing the application of Ga_2O_3 SBDs in high-speed, high-voltage power electronics. Therefore, they have considerable potential for application in β-Ga_2O_3 power devices. Some other related work has also been proposed [195–197].

4.2. PN Heterojunction Diode (HJD)

Although SBDs have the advantage of low V_{ON} and fast recovery times, as compared to p-n junction diodes, and the V_{BR} of β-Ga_2O_3 SBDs can be greatly improved by introducing various termination structures, as mentioned in Section 4.1, it is still challenging to achieve a V_{BR} over 3 kV, which meets the increasing demand for power applications. In addition, the fabrication processes for β-Ga_2O_3 SBDs are always complex. The p-n junction has good electric field management capability, but the efficient realization of intrinsic p-type in β-Ga_2O_3 is a big challenge. The good news is that other p-type oxide semiconductors, such as NiO [198,199], Ir_2O_3 [200,201], SnO [202,203], $CuAlO_2$ [204,205], GaN [206,207], Cu_2O [208,209], Cr_2O_3 [210], etc., can form heterojunctions with β-Ga_2O_3 to make up for the deficiencies of p-type β-Ga_2O_3. The depletion region of the p-n junction can be utilized to regulate the electric field below the anode and suppress the concentration of the electric field at the edge of the Schottky junction, achieving a balance between the high-voltage blocking capability and the low conduction loss. The wide-bandgap NiO has promising potential in power applications due to its structural stability and tunable P doping property. Currently, most of the studies are mainly focusing on NiO/β-Ga_2O_3 pn junction diodes, and the main review in this section is related to the NiO/β-Ga_2O_3 structure heterojunction diodes.

Early in 2017, Watahiki et al. [208] proposed heterojunction p-Cu_2O/n-β-Ga_2O_3 diodes on an epitaxially grown β-Ga_2O_3 (001) layer. The V_{BR} of these p-n diodes reached 1.49 kV with $R_{ON,SP}$ of 8.2 mΩ·cm^2. For the purpose of obtaining higher V_{BR}, in 2020, Lu et al. [211] proposed wide bandgap NiO to form NiO/n-β-Ga_2O_3 heterojunction diodes (HJD), as shown in Figure 12a. For comparison, the Ni/β-Ga_2O_3 SBD is also fabricated. A low $R_{ON,SP}$ of 3.5 mΩ·cm^2 for NiO/β-Ga_2O_3 p-n diodes is achieved as compared to that (4.2 mΩ·cm^2) of Ni/β-Ga_2O_3 SBDs. As shown in Figure 12b, the V_{BR} exceeds 1 kV (1059 V), much higher than that (500 V) of Ni/β-Ga_2O_3 SBD. In order to further improve the power performance of NiO/β-Ga_2O_3 HJD, Gong et al. [212] proposed a bipolar p-NiO structure that consists of a heavily and lightly doped layer. The heavily doped layer can provide high hole concentration, and the lighted doped layer suppresses electric field crowding effectively. In their results, the double-layer diode achieved a high V_{BR} of 1.86 kV as compared to that (0.94 kV) of the single-layer one.

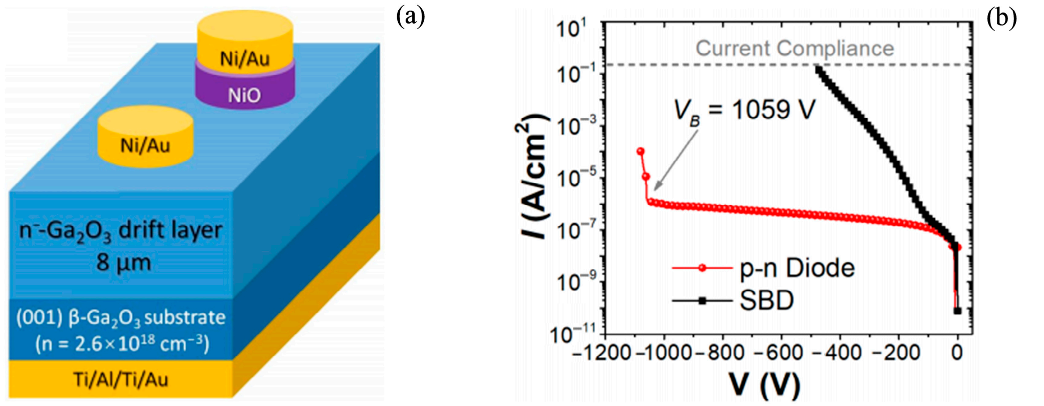

Figure 12. (**a**) Schematic device structures of the vertical NiO/β-Ga_2O_3 heterojunction p-n diode and the Ni/β-Ga_2O_3 SBD; (**b**) comparison of the breakdown characteristics for the NiO/β-Ga_2O_3 heterojunction p-n diode and Ni/β-Ga_2O_3 SBD [211].

In the absence of an optimization field, Hao et al. [198] optimized the interface by annealing. By annealing the interface at 350 °C for 3 min in a N_2 atmosphere, a high-performance NiO/β-Ga_2O_3 p-n diode was obtained. The $R_{ON,SP}$ decreased from 5.4 to 4.1 mΩ·cm^2, and the V_{BR} increased from 900 V to 1630 V with a power quality factor of 0.65 GW/cm^2. The interfacial trap density and current–voltage hysteresis were significantly reduced in their results. In 2025, Liu et al. [199] also proposed an interface optimization technique using O_2 plasma to treat the controllable interface of high-performance NiO_x/β-Ga_2O_3 HJDs. This method significantly improves the device performance by modulating the energy band structure and decreasing the ohmic contact resistance at the Ni/NiO_x interface. Atomic force microscopy (AFM) images demonstrated that a 1 min O_2 plasma treatment resulted in a smoother surface topography, reduced interfacial defects, and improved metal–semiconductor contact quality. The treated HJDs exhibited a significantly higher PFOM of 0.675 GW/cm^2, a 209.63% improvement over the untreated devices. In addition, a high V_{BR} of 1340 V is achieved, superior to most state-of-the-art Ga_2O_3 heterojunction diodes and Schottky barrier diodes without any termination structure. In combination with UV/ozone treatment (UVO), Ding et al. [213] proposed the preparation of NiO_x/β-Ga_2O_3 HJDs with enhanced performance through synergistic interfacial engineering (SIE) with post-annealing processes, which can greatly improve the electrical and interfacial characteristics of HJDs. The results showed that the $R_{ON,SP}$ was 2.47 mΩ·cm^2 with a V_{BR} of 1355 V, resulting in an excellent PFOM of 0.743 GW/cm^2. These studies provide some new strategies for optimizing the metal–semiconductor interface, paving the way for commercialization and scalable fabrication of high-performance β-Ga_2O_3 devices.

Similar to mesa terminal structures, HJDs can also be structured with small angles to reduce electric field concentration and enhance device performance. Zhou et al. [214] fabricated large-area (1 × 1 mm^2) small-angle (∼11°) beveled NiO/β-Ga_2O_3 HJDs, as shown in Figure 13a. The fabricated HJDs exhibit a static V_{BR} of 1.95 kV and a dynamic V_{BR} of 2.23 kV, with an $R_{ON,SP}$ of 1.9 mΩ·cm^2. Subsequently, they fabricated HJDs [215] with a 6° tilt angle, giving a V_{BR} of up to 2.04 kV. The device had a measured $R_{ON,SP}$ of 2.26 mΩ·cm^2 and a PFOM of 1.84 GW/cm^2 at DC. The device showed a V_{BR} of 1.23 kV at 200 °C, exhibiting high thermal stability. In addition, the extension of NiO material has the advantage of reducing the electric field crowding at the edges of the diode [216], which results in the device's V_{BR} of 4.7 kV and an $R_{ON,SP}$ of 11.3 mΩ·cm^2, with a PFOM reaching 2 GW/cm^2. The effect has also been studied and verified by other groups [217–219].

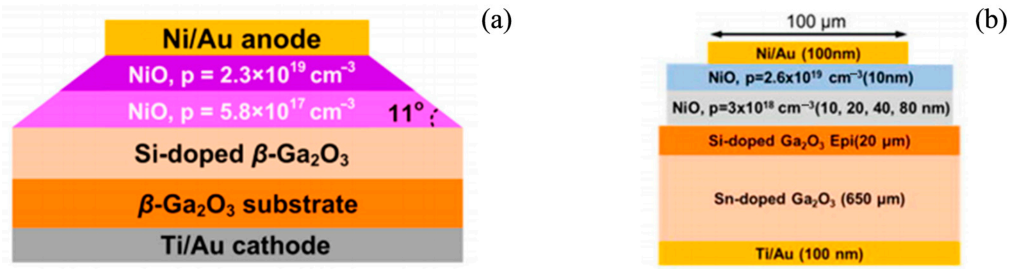

Figure 13. Schematic cross-sectional view of the beveled mesa NiO/β-Ga_2O_3 HJD (**a**) [214]; NiO/β-Ga_2O_3 HJD with JTE (**b**).

The performance of HJDs can be further improved by combining with other techniques. In 2024, Wan et al. [220] etched ~7 μm deep trenches to reduce the anode edge electric field using a self-alignment technique. The trenches with SiO_2/PI/SiO_2 dielectric structures and additional field plates were added. The deep trench terminations and the field plates alleviate the electric field crowding around the junction. The fabricated SBDs exhibit an enhanced V_{BR} of 2050 V as compared to other structures in their results. In 2025, Wan et al. [5] proposed a p-type NiO material encapsulated in a deep countertop using a termination method as an RESURF structure. This structure does not require a self-alignment process, which expands the flexibility of the termination design and reduces the influence of dielectric charge on the effectiveness of the edge termination. The fabricated device exhibits the high V_{BR} of 3214 V, $R_{ON,SP}$ of 4.05 mΩ·cm^2, and PFOM of 2.55 GW/cm^2. The technique provides a versatile and effective edge termination solution for β-Ga_2O_3 power devices. In 2025, Jia et al. [221] prepared p-type NiO on n-β-Ga_2O_3 epitaxial layers by sputtering and effectively suppressed the electric field at the p-n junction of the device by He ion implantation as a highly efficient and low-damage edge termination. The V_{BR} was enhanced from 1330 V to 3000 V, the $R_{ON,SP}$ was 3.12 mΩ·cm^2, and the PFOM was 2.88 GW/cm^2. This study provides a new idea for the design and fabrication of high-power, low-loss β-Ga_2O_3 bipolar power devices. Also, some other related works have been reported [222–228], aiming to improve the NiO/β-Ga_2O_3 SBD performance.

In summary, heterojunction p-n diodes have become the core solution for balancing V_{BR} and conduction loss in β-Ga_2O_3 power devices through interface engineering and termination structure innovation. In particular, the bilayer NiO design and composite termination technology have realized over 3 kV breakdown voltage, showing the potential to surpass SiC/GaN. In the future, we need to focus on material compatibility and large-area process optimization to promote its commercialization in ultra-high-voltage power transmission and high-temperature power electronics scenarios.

4.3. Heterojunction Barrier Schottky (HJBS) Diodes

The HJBS diode structure utilizes p-type oxides (e.g., NiO and SnO) and n-type β-Ga_2O_3 to form a heterojunction, which achieves low-voltage conduction through the Schottky junction in forward bias and suppresses the edge field concentration with the help of a pn junction depletion region in reverse bias, which combines high efficiency rectification with high blocking capability. The research progress of β-Ga_2O_3 HJBS in recent years is summarized below.

In 2021, Lv et al. [229] reported the early Ga_2O_3 HJBS diode, as shown in Figure 14a. The p-NiO was formed using a Ni thermally oxidized method. In their results, the small-area β-Ga_2O_3 HJBS diode demonstrated a high V_{BR} of 1715 V and low $R_{ON,SP}$ of 3.45 mΩ·cm^2, resulting in the highest dc FOM = 0.85 GW/cm^2. This method provides guidance for balancing the turn-on capability and leakage current suppression of Ga_2O_3 power devices. In 2022, Yan et al. [230] etched the Ga_2O_3 surface to form fin structures. After that, sputtered p-NiO was used to realize the HJBS structure. In their results, the leakage current was minimized by the p-NiO fins. The HJBS exhibited a low $R_{ON,SP}$ of 1.94 mΩ·cm^2 and a V_{BR} of 1.34 kV with a fin width of 3 μm, exhibiting a high DC PFOM of 0.93 GW·cm^{-2}. In 2023, Zhang et al. [231], for the first time, compared the performance of 1 mm^2 NiOx/β-Ga_2O_3 HJBS diodes with strip and honeycomb anode p$^+$ island layouts using 3D TCAD simulations. The results show that the cellular layout HJBS diode has slightly higher on-state voltage and resistance, but the V_{BR} increases from 412 V to 567 V, a 38% improvement, the BFOM increases by 59%, and the reverse leakage current decreases by two orders of magnitude. Both devices have similar reverse recovery, with t_{rr} on the order of nanoseconds. In addition, the cellular HJBS diode provides better inrush current robustness, thanks to better heat dissipation. These results indicate that the honeycomb structure can further improve the power performance of NiO_x/β-Ga_2O_3 HJBS diodes with great potential for power applications. In 2025, Wang et al. [232] prepared β-Ga_2O_3 HJBS diodes by reactive magnetron sputtering selective growth of circular p-type SnO thin film arrays in combination with β-Ga_2O_3 substrates. The SnO/β-Ga_2O_3 HJBS diode showed suppressed reverse leakage currents due to the reduced crowding effect of the electric field at the anode edges and the transverse depletion effect of p-n junctions, resulting in an increase in V_{BR}. The device was shown to have a turn-on voltage of 1.2 V, an $R_{ON,SP}$ of 5.1 mΩ·cm^2, a V_{BR} up to 1375 V, a Baliga power quality factor of 0.37 GW/cm^2, and a reverse leakage current of less than 2 μA/cm^2 when reverse biased to 1250 V. The performance of HJBS diodes with different pitches is also investigated, showing that the reduction in pitch is expected to further improve the V_{BR}, and the diodes have a promising application in future β-Ga_2O_3 power electronic devices. Hu et al. [233] simplified the fabrication process of β-Ga_2O_3-based HJBS diodes by utilizing self-assembled nickel nanostructures as in situ masks, as shown in Figure 14b. A Ga_2O_3 HJBS power diode without alignment was demonstrated with a trench depth of 200 nm, and the device's inverse characteristics shifted from a conventional SBD to a p-n bipolar structure. The transverse pinch-off effect redistributes the electric field, reducing the reverse leakage current density by 108 A/cm^2 (reverse bias 100 V). In addition, the V_{BR} increases by 748 V while retaining the forward conduction advantage of low on-resistance, providing a simple strategy to simplify the fabrication process of Ga_2O_3-based HJBS diodes. Gong et al. [234] prepared NiO/β-Ga_2O_3 p-n heterojunction diodes with a room-temperature reactive sputtering technique without any etching process, effectively avoiding intentional etching damage. The HJBS diodes with a uniform FLR width/spacing of 2 μm achieved a maximum V_{BR} of 1.89 kV and an $R_{ON,SP}$ of 7.7 mΩ·cm^2, with a Baliga quality factor of 0.46 GW/cm^2, as shown in Figure 14c.

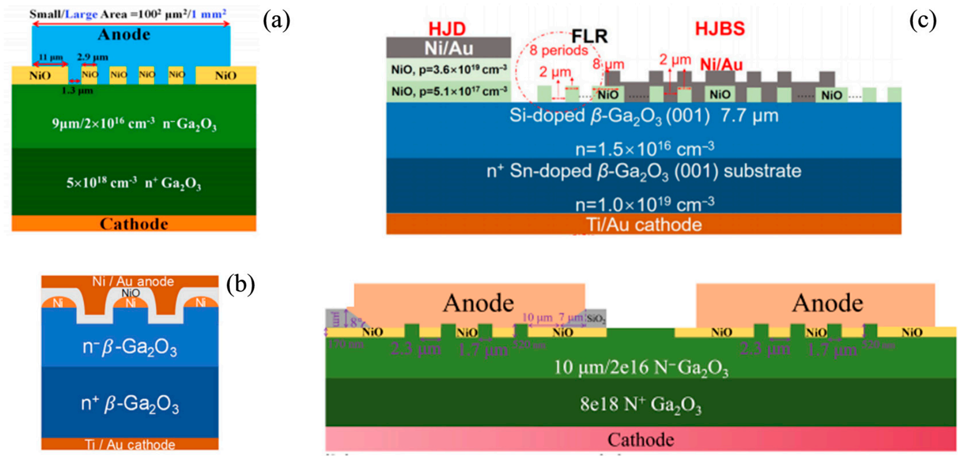

Figure 14. Schematic cross-sectional view of (**a**) the Ga_2O_3 HJBS diodes with thermally oxidized p-NiO [229]; (**b**) the self-aligned HJB diode [233]; (**c**) HJB diode with p-NiO FLRs [234]; (**d**) the Ga_2O_3 JBS diode with field plate structure (left) and without beveled field plate (right) [154].

Combined with the field plate technique, the performance of NiO/β-Ga_2O_3 HJBS can be further improved [154,235]. In 2023, Wei et al. [154] inserted a small-angle (~8°) SiO_2 field plate on the edge of NiO/β-Ga_2O_3 HJBS diodes, as shown in Figure 14d, increasing the V_{BR} from 1895 V to 2395 V, achieving a PFOM of 0.72 GW with the small-scale (0.1×0.1 mm^2) diode.

Despite the challenges of material thermal mismatch and large-area processes, HJBS, with its low-cost and easy-to-integrate features, shows potential to surpass SiC/GaN in ultra-high-voltage transmission and high-temperature power electronics. In the future, efforts should be focused on the optimization of new p-type materials and atomic layer deposition processes to accelerate the industrialization process.

4.4. Lateral Structure Diodes

Although lateral devices have a larger area compared to vertical ones, they have the advantage of low cost and improved thermal dissipation by integrating with other substrates. Lateral structure, without the need for substrate thinning, backside metallization, and other complex processes, is more convenient to integrate with other power devices (such as MOSFETs and IGBTs) or drive circuits to achieve monolithic integration to reduce the complexity of the system-level packaging.

In 2018, Hu et al. [236] reported the first high-performance lateral β-Ga_2O_3 SBD on a sapphire substrate. The β-Ga_2O_3 nano-membrane channel was transformed from a low dislocation density bulk β-Ga_2O_3 substrate to a sapphire substrate. The fabricated SBDs with a Schottky–ohmic contact distance of 15 μm exhibit the high V_{BR} of 1.7 kV in their results, even without being field plate assisted. Subsequently, combined with the field plate technique, researchers [237] reported lateral β-Ga_2O_3 SBDs with a V_{BR} over 3 kV when anode to cathode spacing (L_{AC}) = 24 or 31 μm for the first time. When L_{AC} = 16 μm, they fabricated the lateral SBDs with a V_{BR} of 2.25 kV, a record DC PFOM of 500 MW/cm^2 at that time. The device's structure can be seen in Figure 15a. In 2023, as shown in Figure 15b, by combining a dual-field plate structure with a post-anode deposition annealing (PAA) treatment technique, which effectively suppressed the interfacial density of states, Chen et al. [238] for the first time, fabricated the lateral β-Ga_2O_3 SBDs with V_{BR} increasing from about 4 kV to more than 10 kV with L_{AC} = 90 μm. The turn-on voltage was kept at about 1 V.

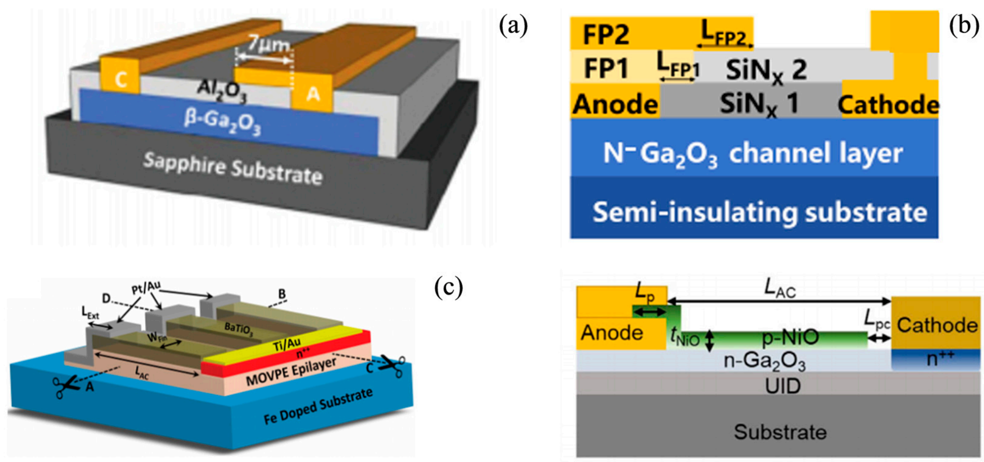

Figure 15. Schematic cross-sectional view of (**a**) the lateral β-Ga_2O_3 SBDs with field plate structure [237]; (**b**) the lateral 10-kV Ga_2O_3 SBD with double FP anode engineered technique [238]; (**c**) the Ga_2O_3 lateral trenched SBD with high-k dielectric superjunction [239]; (**d**) the 10 kV β-Ga_2O_3 SBDs with RESURF termination [240].

In 2022, Roy et al. [239] realized high-k ($BaTiO_3$) transverse trench superjunction (SJ) lateral β-Ga_2O_3 SBDs on an epilayer with a sheet charge of 1.5×10^{13} cm^{-2}, as shown in Figure 15c. When the anode-to-cathode distance was 5 μm, they achieved lateral SBDs with $R_{ON,SP}$ of 1.65 mΩ·cm^2, V_{BR} of 1487 V, and PFOM of 1.34 GW/cm^2, which provides a new solution for the development of β-Ga_2O_3-based power devices and is expected to promote their development in multi-kilovolt applications.

In addition, in 2023, Yuan et al. [240] designed a novel transverse Ga_2O_3 SBD, as shown in Figure 15d, which employs a reduced surface electric field structure (RESURF) of p-type NiO to achieve breakdown voltages (>10 KV) at high temperatures of up to 200 °C. The fabricated SBD shows an $R_{ON,SP}$ of 0.27 Ω·cm^2 and a turn-on voltage of 1 V. The results in their work suggest that the Ga_2O_3 device has a high voltage in medium- and high-voltage, high-temperature power applications with good potential.

In 2024, Cho et al. [241] prepared transverse SBDs on Si-doped β-Ga_2O_3 wafers grown by molecular beam epitaxy (MBE) with different anode and cathode spacings of the devices and an anode-connected field plate structure. The effects of different spacings and field plate structures on the device's performance were investigated. Their results exhibited a near-zero turn-on voltage, sub-60 mV/dec subthreshold swing, and high V_{BR} of 3694 V. However, due to the ohmic contacting process, the on-resistance of the device was high, resulting in a PFOM of only 18.87 MW/cm^2. The ohmic contacting process can be optimized later on to reduce the on-resistance and improve the PFOM. Some other lateral structure β-Ga_2O_3 diodes have also been proposed and studied [242–245].

4.5. Other Representative SBDs

Junction termination extension (JTE) structures homogenize the electric field distribution by introducing lightly doped p-type regions at the edge of the main junction, allowing the depletion region to extend toward the device edge and avoiding premature breakdown due to the concentration of the electric field. The structure can be realized by ion implantation or thin film growth without complex multilayer dielectric deposition or high-precision etching, combining process compatibility and E-field regulation efficiency.

In 2022, as shown in Figure 16a, Hao et al. [246] used a sputtering process to adjust the charge concentration of p-type NiO as the JTE, which can effectively suppress the main junction edge electric field. A reasonable charge concentration in the JTE region can balance the main Schottky junction and the edge electric field in the JTE region. The results show that the $R_{ON,SP}$ is 2.9 mΩ/cm^2, the V_{BR} is 2.11 kV, and the power quality factor is 1.54 GW/cm^2. By using multiple layers of p-NiO JTE, Wang et al. [247] fabricated β-Ga_2O_3 SBDs that showed an $R_{ON,SP}$ of 5.9 mΩ/cm^2, a V_{BR} of greater than 2.5 kV, and a PFOM surpassing 1 GW/cm^2. In 2025, Chang et al. [114] prepared fully vertical β-Ga_2O_3 JTE-SBDs using sputtered p-GaN layers to solve the p-Ga_2O_3 material deficiency problem, as shown in Figure 15b. The device has a turn-on voltage of 0.8 V, an $R_{ON,SP}$ of 6.15 mΩ·cm^2, a V_{BR} of 3 kV, and a Baliga quality factor of 1.46 GW/cm^2. The p-GaN layer preparation process can be further optimized to improve the device performance. Some other β-Ga_2O_3 SBDs JTE techniques can be seen in Refs. [248–251].

Gong et al. [252] fabricated a high-performance Ga_2O_3 vertical HJBS diode by integrating a TiN/Ga_2O_3 Schottky contact, p-NiO-filled trenches, and p-NiO field-limited loops. Using an embedded p-type NiO lattice to move the peak electric field away from the Schottky junction, thus permitting the use of an ultra-low-barrier TiN Schottky contact, the HJBS achieved a low on-state voltage of 0.91 V and a high V_{BR} of more than 1 kV. In the study of Ref. [253], Han proposed β-Ga_2O_3 SBDs with composite termination that combines mesa and gradual junction termination extension (MJTE). By optimizing the device's parameters, the V_{BR} increased from 738 V to 2116 V, resulting in a huge improvement in the PFOM to 608.35 MW/cm^2. In 2024, Prajapati et al. [254] reported, for the first time, the use of interfacial dipoles to modulate the Schottky barrier height (SBH) of β-Ga_2O_3 SBDs, and a significant enhancement of the SBH and V_{BR} was achieved by the ultrathin plasma-enhanced atomic layer deposition-prepared (PEALD) AlO_x interfacial layer. In their results, the AlO_x layer does not significantly increase the on-resistance, and the 5 Å thick AlOx layer has the best effect with the highest enhancement of SBH of 0.8 eV and V_{BR} up to nearly 500 V. In the same year, Hong et al. [104] used AlN as the interface material prepared by an atomic layer deposition (AlD) process. Compared with conventional β-Ga_2O_3 SBDs, the AlN/β-Ga_2O_3 MIS SBDs have three orders of magnitude lower reverse leakage currents and higher V_{BR}, from 208 V to 890 V, while maintaining a relatively low V_{ON} of 0.92 V and an $R_{ON,SP}$ of 11.8 mΩ·cm^2. These two studies provide new approaches to enhance the performance of β-Ga_2O_3 SBDs. In 2023, as shown in Figure 16c, Qin et al. [255] fabricated vertical superjunction Schottky barrier diodes (SJ-SBDs) by integrating p-NiO within the trenches of β-Ga_2O_3. The fabricated devices exhibited an $R_{ON,SP}$ of only 0.7 mΩ·cm^2, and V_{BR} exceeded 2000 V.

Also, in 2023, Hendricks et al. [227] proposed metal dielectric semiconductor (MDS) diodes with a TiO_2 interlayer, which achieved lower turn-on voltage and similar $R_{ON,SP}$, while reducing reverse leakage current. Compared with conventional SBDs, the on-state voltage was reduced from 0.88 V to 0.59 V, and the V_{BR} was improved from 548 V to 1380 V. They then investigated the current transport mechanism of the device, showing that electron emission is a good description of the current in forward and reverse bias. The results show that tunneling currents are greatly suppressed, so that a diode sandwiched with titanium dioxide can block more current than a Schottky barrier diode by orders of magnitude with the same barrier height. Finally, a 1200 V diode structure is designed based on the derived transport model, and the calculated on-state and off-state current characteristics are very close to those of the latest commercial 4 H-SiC devices, indicating that the diode structure can realize a β-Ga_2O_3 power diode [256].

In addition, as shown in Figure 16d, Li et al. [257] proposed the preparation of β-Ga_2O_3 SBDs with a Mg current blocking layer (Mg-CBL) by a Mg-doped spin-coated glass (Mg-SOG) technique, which realizes the thermal doping process without surface roughness damage. The Mg-CBL traps the electrons, mitigates the electric field, and reduces the reverse saturation current; the V_{BR} increased from 580 V to 2200 V, $R_{ON,SP}$ increased from 4.0 to 4.8 mΩ·cm^2, and the power quality factor exceeded 1 GW/cm^2.

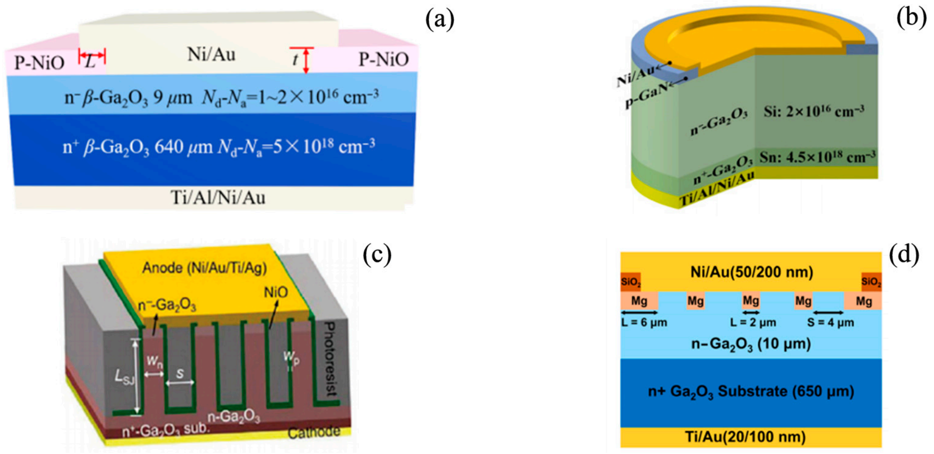

Figure 16. Schematic cross-sectional view of (**a**) the lateral β-Ga_2O_3 SBDs with single-zone p-NiO JTE [246]; (**b**)the fabrication process for p-GaN/n-Ga_2O_3 JTE-SBD [114]; (**c**) the superjunction SBD [255]; (**d**) the proposed β-Ga_2O_3 SBD with Mg-SOG CBL [257].

5. Conclusions and Outlooks

The research progress of different structures of β-Ga_2O_3 power diodes includes vertical and lateral structures with various advanced techniques. For SBDs, field plate techniques can redistribute the electric field to reduce the localized electric field intensity, enhancing the V_{BR}. FP oxide material, the thickness, multiple-layer FP, FP angle, and FP length are optimized for improving the device's electrical performance. As for the ET technique, ion implantation and oxygen annealing are two of the main methods of forming a high-resistivity region. N, Ar, F, He, and Mg are always selected to form ion implantation terminals, and the annealing temperature should be optimized. For trench MOS SBD, the dimensions and shape, fabrication process, epitaxial layer doping concentration, and fin channel orientation should be carefully designed and selected. For pn junction diodes, NiO/β-Ga_2O_3 is always selected and exhibits excellent performance. Post-annealing, the NiO layer angle, the NiO growth method, and the NiO extension are factors that affect the device's performance. For HJBS, p-type materials, the growth method, and dimensions should be considered.

For β-Ga_2O_3 diodes, SBDs usually have a lower V_{ON}, with V_{BR} not as high as that of pn junction diodes. Ion implantation ET techniques or HJBS diodes can remedy this issue, but the fabrication cost is much higher. pn junction (HJD) and HJBS diodes are promising for achieving high V_{BR}. However, HJBS diodes suffer from much greater structure complexity. SJ diodes usually exhibit the best trade-off between low V_{ON} and high V_{BR}.

In this work, the β-Ga_2O_3 power diode technique has been discussed comprehensively, including vertical and lateral structures with various advanced techniques. Although state-of-the-art techniques for fabricating β-Ga_2O_3 power diodes have been proposed and summarized in this work, there is still significant room for exploration to improve β-Ga_2O_3 power diodes' performance. In summary, β-Ga_2O_3 power diode techniques will continue to be a research focus for power applications in the future. We believe the content presented in this work will be beneficial for understanding and achieving high-performance β-Ga_2O_3 power diodes.

Author Contributions: L.-Q.Z.: writing—original draft, investigation, data curation, and conceptualization; J.-J.L., Y.-T.T., H.X., Q.-H.Y. and H.-F.L.: writing—original draft, investigation, data curation, and conceptualization; Z.-Y.W. and L.-F.S.: writing—review and editing, visualization, and validation. All authors have read and agreed to the published version of the manuscript.

Funding: This work was supported in part by the Science and Technology Project of Henan Province under No. 242102210168, Key scientific research projects of higher education institutions in Henan Province under No. 25A510005, and Henan Province Natural Science Foundation project No. 252300420330.

Data Availability Statement: Not applicable.

Conflicts of Interest: The authors declare no conflicts of interest.

References

1. Xiong, Y.; Sadek, M.; Chu, R. Recent advances in GaN-based power devices, and integration. *Semicond. Sci. Technol.* **2025**, *40*, 033002. [CrossRef]
2. Buffolo, M.; Favero, D.; Marcuzzi, A.; De Santi, C.; Meneghesso, G.; Zanoni, E.; Meneghini, M. Review and Outlook on GaN and SiC Power Devices: Industrial State-of-the-Art, Applications, and Perspectives. *IEEE Trans. Electron Devices* **2024**, *71*, 1344–1355. [CrossRef]
3. Nielsen, M.R.; Deng, S.; Mirza, A.B.; Kjærsgaard, B.F.; Jørgensen, A.B.; Zhao, H.; Li, Y.; Munk-Nielsen, S.; Luo, F. High-Power Electronic Applications Enabled by Medium Voltage Silicon-Carbide Technology: An Overview. *IEEE Trans. Power Electron.* **2024**, *40*, 987–1011. [CrossRef]
4. Herath Mudiyanselage, D.; Da, B.; Adivarahan, J.; Wang, D.; He, Z.; Fu, K.; Zhao, Y.; Fu, H. β-Ga_2O_3-based heterostructures and heterojunctions for power electronics: A review of the recent advances. *Electronics* **2024**, *13*, 1234. [CrossRef]
5. Wan, J.; Wang, H.; Zhang, C.; Wang, C.; Cheng, H.; Ye, J.; Zhang, Y.; Sheng, K. Junction-based deep mesa termination for multi-kilovolt vertical β-Ga_2O_3 power devices. *Appl. Phys. Lett.* **2025**, *126*, 032106. [CrossRef]
6. Wu, F.; Wen, J.; Liu, J.; Li, Q.; Han, Z.; Hao, W.; Zhou, X.; Xu, G.; Long, S. Reliability of 1.5 $\times$ 1.5 mm^2 β-Ga_2O_3 Power Diodes and Application in DC-DC Converter. *Phys. Status Solidi B* **2025**, *262*, 2400438. [CrossRef]
7. Sun, S.; Wang, C.; Alghamdi, S.; Zhou, H.; Hao, Y.; Zhang, J. Recent advanced ultra-wide bandgap β-Ga_2O_3 material and device technologies. *Adv. Electron. Mater.* **2025**, *11*, 2300844. [CrossRef]
8. Reddy, M.N.; Panda, D.K. Next Generation High-Power Material Ga_2O_3: Its Properties, Applications, and Challenges. In *Nanoelectronic Devices and Applications*; Bentham Books: Sharjah, United Arab Emirates, 2024; pp. 160–188.
9. Taboada Vasquez, J.M.; Li, X. A Review of Vertical Ga_2O_3 Diodes: From Fabrication to Performance Optimization and Future Outlooks. *Phys. Status Solidi B* **2025**, *262*, 2400635. [CrossRef]
10. Higashiwaki, M. Gallium Oxide Power Electronics: The Key Semiconductor for Realizing Energy Sustainable Future. *IEEE Electron. Devices Mag.* **2025**, *2*, 42–48. [CrossRef]
11. Pearton, S.J.; Yang, J.; Cary, P.H.; Ren, F.; Kim, J.; Tadjer, M.J.; Mastro, M.A. A review of Ga_2O_3 materials, processing, and devices. *Appl. Phys. Rev.* **2018**, *5*, 011301. [CrossRef]
12. Higashiwaki, M.; Murakami, H.; Kumagai, Y.; Kuramata, A. Current status of Ga_2O_3 power devices. *Jpn. J. Appl. Phys.* **2016**, *55*, 1202A1. [CrossRef]
13. Galazka, Z.; Uecker, R.; Klimm, D.; Irmscher, K.; Naumann, M.; Pietsch, M.; Kwasniewski, A.; Bertram, R.; Ganschow, S.; Bickermann, M. Scaling-up of bulk β-Ga_2O_3 single crystals by the Czochralski method. *ECS J. Solid State Sci. Technol.* **2016**, *6*, 3007–3011. [CrossRef]
14. Kuramata, A.; Koshi, K.; Watanabe, S.; Yamaoka, Y.; Masui, T.; Yamakoshi, S. High-quality β-Ga_2O_3 single crystals grown by edge-defined film-fed growth. *Jpn. J. Appl. Phys.* **2016**, *55*, 1202A2. [CrossRef]
15. Hoshikawa, K.; Ohba, E.; Kobayashi, T.; Yanagisawa, J.; Miyagawa, C.; Nakamura, Y. Growth of β-Ga_2O_3 single crystals using vertical Bridgman method in ambient air. *J. Cryst. Growth* **2016**, *447*, 36–41. [CrossRef]
16. Nikolaev, V.I.; Maslov, V.; Stepanov, S.I.; Pechnikov, A.I.; Krymov, V.; Nikitina, I.P.; Guzilova, L.I.; Bougrov, V.E.; Romanov, A.E. Growth and characterization of β-Ga_2O_3 crystals. *J. Cryst. Growth* **2017**, *457*, 132–136. [CrossRef]
17. Víllora, E.G.; Shimamura, K.; Yoshikawa, Y.; Aoki, K.; Ichinose, N. Large-size β-Ga_2O_3 single crystals and wafers. *J. Cryst. Growth* **2004**, *270*, 420–426. [CrossRef]
18. Aida, H.; Nishiguchi, K.; Takeda, H.; Aota, N.; Sunakawa, K.; Yaguchi, Y. Growth of β-Ga_2O_3 single crystals by the edge-defined, film fed growth method. *Jpn. J. Appl. Phys.* **2008**, *47*, 8506. [CrossRef]
19. Zhang, J.; Li, B.; Xia, C.; Pei, G.; Deng, Q.; Yang, Z.; Xu, W.; Shi, H.; Wu, F.; Wu, Y.; et al. Growth and spectral characterization of β-Ga_2O_3 single crystals. *J. Phys. Chem. Solids* **2006**, *67*, 2448–2451. [CrossRef]
20. Ohba, E.; Kobayashi, T.; Taishi, T.; Hoshikawa, K. Growth of (100), (010) and (001) β-Ga_2O_3 single crystals by vertical Bridgman method. *J. Cryst. Growth* **2021**, *556*, 125990. [CrossRef]
21. Fu, B.; Jian, G.; Mu, W.; Li, Y.; Wang, H.; Jia, Z.; Li, Y.; Long, S.; Shi, Y.; Tao, X. Crystal growth and design of Sn-doped β-Ga_2O_3: Morphology, defect and property studies of cylindrical crystal by EFG. *J. Alloys Compd.* **2022**, *896*, 162830. [CrossRef]
22. Galazka, Z. Growth of bulk β-Ga_2O_3 single crystals by the Czochralski method. *J. Appl. Phys.* **2022**, *131*, 031103. [CrossRef]

23. Meng, L.; Feng, Z.; Bhuiyan, A.A.U.; Zhao, H. High-mobility MOCVD β-Ga_2O_3 epitaxy with fast growth rate using trimethylgallium. *Cryst. Growth Des.* **2022**, *22*, 3896–3904. [CrossRef]
24. Leach, J.H.; Udwary, K.; Rumsey, J.; Dodson, G.; Splawn, H.; Evans, K.R. Halide vapor phase epitaxial growth of β-Ga_2O_3 and α-Ga_2O_3 films. *APL Mater.* **2019**, *7*, 022504. [CrossRef]
25. Blumenschein, N.; Paskova, T.; Muth, J. Effect of Growth Pressure on PLD-Deposited Gallium Oxide Thin Films for Deep-UV Photodetectors. *Phys. Status Solidi A* **2019**, *216*, 1900098. [CrossRef]
26. Garten, L.M.; Zakutayev, A.; Perkins, J.D.; Gorman, B.P.; Ndione, P.F.; Ginley, D.S. Structure property relationships in gallium oxide thin films grown by pulsed laser deposition. *MRS Commun.* **2016**, *6*, 348–353. [CrossRef]
27. Xiu, X.; Zhang, L.; Li, Y.; Xiong, Z.; Zhang, R.; Zheng, Y. Application of halide vapor phase epitaxy for the growth of ultra-wide band gap Ga_2O_3. *J. Semicond.* **2019**, *40*, 011805. [CrossRef]
28. Khartsev, S.; Nordell, N.; Hammar, M.; Purans, J.; Hallén, A. High-Quality Si-Doped β-Ga_2O_3 Films on Sapphire Fabricated by Pulsed Laser Deposition. *Phys. Status Solidi B* **2021**, *258*, 2000362. [CrossRef]
29. Gogova, D.; Wagner, G.; Baldini, M.; Schmidbauer, M.; Irmscher, K.; Schewski, R.; Galazka, Z.; Albrecht, M.; Fornari, R. Structural properties of Si-doped β-Ga_2O_3 layers grown by MOVPE. *J. Cryst. Growth* **2014**, *401*, 665–669. [CrossRef]
30. Sood, A.; Wuu, D.S.; Tarntair, F.G.; Sao, N.T.; Wu, T.L.; Tumilty, N.; Kuo, H.C.; Pratap, S.J.; Horng, R.H. Electrical performance study of Schottky barrier diodes using ion implanted β-Ga_2O_3 epilayers grown on sapphire substrates. *Mater. Today Adv.* **2023**, *17*, 100346. [CrossRef]
31. Kyrtsos, A.; Matsubara, M.; Bellotti, E. On the feasibility of p-type Ga_2O_3. *Appl. Phys. Lett.* **2018**, *112*, 032108. [CrossRef]
32. Lyons, J.L. A survey of acceptor dopants for β-Ga_2O_3. *Semicond. Sci. Technol.* **2018**, *33*, 05LT02. [CrossRef]
33. Wong, M.H.; Lin, C.H.; Kuramata, A.; Yamakoshi, S.; Murakami, H.; Kumagai, Y.; Higashiwaki, M. Acceptor doping of β-Ga_2O_3 by Mg and N ion implantations. *Appl. Phys. Lett.* **2018**, *113*, 102103. [CrossRef]
34. Su, Y.; Guo, D.; Ye, J.; Zhao, H.; Wang, Z.; Wang, S.; Li, P.; Tang, W. Deep level acceptors of Zn-Mg divalent ions dopants in β-Ga_2O_3 for the difficulty to p-type conductivity. *J. Alloys Compd.* **2019**, *782*, 299–303. [CrossRef]
35. Li, L.; Liao, F.; Hu, X. The possibility of N-P codoping to realize P type β-Ga_2O_3. *Superlattices Microstruct.* **2020**, *141*, 106502. [CrossRef]
36. Kananen, B.E.; Giles, N.C.; Halliburton, L.E.; Foundos, G.K.; Chang, K.B.; Stevens, K.T. Self-trapped holes in β-Ga_2O_3 crystals. *J. Appl. Phys.* **2017**, *122*, 215703. [CrossRef]
37. Gake, T.; Kumagai, Y.; Oba, F. First-principles study of self-trapped holes and acceptor impurities in Ga_2O_3 polymorphs. *Phys. Rev. Mater.* **2019**, *3*, 044603. [CrossRef]
38. Zhu, Z.; Yan, T.; Tian, H.; Lai, J.; Wang, C.; Chen, C.; Luo, M. Epitaxial Growth of p-Type Cu-Doped Ga_2O_3 Nanoarrays on MgO Substrates. *Cryst. Growth Des.* **2024**, *24*, 4443–4450. [CrossRef]
39. Zeng, K.; Bian, Z.; Sinha, N.; Chowdhury, S. Simultaneous drive-in of Mg and disassociation of Mg-H complex in Ga_2O_3 by oxygen annealing achieving remarkable current blocking. *Appl. Phys. Lett.* **2024**, *124*, 212102. [CrossRef]
40. Saha, S.; Meng, L.; Bhuiyan, A.F.M.A.U.; Sharma, A.; Saha, C.N.; Zhao, H.; Singisetti, U. Electrical characteristics of in situ Mg-doped β-Ga_2O_3 current-blocking layer for vertical devices. *Appl. Phys. Lett.* **2023**, *123*, 132105. [CrossRef]
41. Labed, M.; Park, B.I.; Kim, J.; Park, J.H.; Min, J.Y.; Hwang, H.J.; Kim, J.; Rim, Y.S. Ultrahigh photoresponsivity of W/Graphene/β-Ga_2O_3 Schottky barrier deep ultraviolet photodiodes. *ACS Nano* **2024**, *18*, 6558–6569. [CrossRef]
42. Zhang, N.; Wang, Z.; Lin, Z.; Zhu, S.; Cai, W.; Zhang, L.; Zhang, X.; Rong, M.; Zhang, X.; Chen, D.; et al. β-Ga_2O_3 extreme ultraviolet photodetectors. *Eur. Phys. J. Spec. Top.* **2025**, *234*, 303–309. [CrossRef]
43. Fang, C.; Li, T.; Shao, Y.; Wang, Y.; Hu, H.; Yang, J.; Zeng, X.; Li, X.; Wang, D.; Ding, Y.; et al. High-performance solar-blind ultraviolet photodetectors based on a Ni/β-Ga_2O_3 vertical Schottky barrier diode. *Nano Lett.* **2025**, *25*, 914–921. [CrossRef]
44. Furthmüller, J.; Bechstedt, F. Quasiparticle bands and spectra of Ga_2O_3 polymorphs. *Phys. Rev. B* **2016**, *93*, 115204. [CrossRef]
45. Cora, I.; Mezzadri, F.; Boschi, F.; Bosi, M.; Čaplovičová, M.; Calestani, G.; Dódony, I.; Pécz, B.; Fornari, R. The real structure of ε-Ga_2O_3 and its relation to κ-phase. *CrystEngComm* **2017**, *19*, 1509–1516. [CrossRef]
46. Qin, Y.; Li, L.; Zhao, X.; Tompa, G.S.; Dong, H.; Jian, G.; He, Q.; Tan, P.; Hou, X.; Zhang, Z.; et al. Metal-semiconductor-metal ε-Ga_2O_3 solar-blind photodetectors with a record-high responsivity rejection ratio and their gain mechanism. *ACS Photonics* **2020**, *7*, 812–820. [CrossRef]
47. Hu, Y.; Zhang, L.; Chen, T.; Ma, Y.; Tang, W.; Huang, Z.; Li, B.; Xu, K.; Mudiyanselage, D.H.; Fu, H.; et al. High-performance ε-Ga_2O_3 solar-blind ultraviolet photodetectors on Si (100) substrate with molybdenum buffer layer. *Vacuum* **2023**, *213*, 112130. [CrossRef]
48. Qian, H.; Zhang, X.; Ma, Y.; Zhang, L.; Chen, T.; Wei, X.; Tang, W.; Zhou, X.; Feng, B.; Fan, Y.; et al. Quasi-vertical ε-Ga_2O_3 solar-blind photodetectors grown on p-Si substrates with Al_2O_3 buffer layer by metalorganic chemical vapor deposition. *Vacuum* **2022**, *200*, 111019. [CrossRef]
49. Fei, Z.; Chen, Z.; Chen, W.; Luo, T.; Chen, S.; Liang, J.; Wang, X.; Lu, X.; Wang, G.; Pei, Y. High-performance ε-Ga_2O_3 solar-blind photodetectors grown by MOCVD with post-thermal annealing. *Coatings* **2023**, *13*, 1987. [CrossRef]

50. Liu, Z.; Huang, Y.; Li, H.; Zhang, C.; Jiang, W.; Guo, D.; Wu, Z.; Li, P.; Tang, W. Fabrication and characterization of Mg-doped ε-Ga_2O_3 solar-blind photodetector. *Vacuum* **2020**, *177*, 109425. [CrossRef]
51. Zhou, S.; Zheng, Q.; Yu, C.; Huang, Z.; Chen, L.; Zhang, H.; Li, H.; Xiong, Y.; Kong, C.; Ye, L.; et al. A high-performance ε-Ga_2O_3 -based deep-ultraviolet photodetector array for solar-blind imaging. *Materials* **2022**, *16*, 295. [CrossRef]
52. Zhang, W.; Wang, W.; Zhang, J.; Zhang, T.; Chen, L.; Wang, L.; Zhang, Y.; Cao, Y.; Ji, L.; Ye, J. Directional carrier transport in micrometer-thick gallium oxide films for high-performance deep-ultraviolet photodetection. *ACS Appl. Mater. Interfaces* **2023**, *15*, 10868–10876. [CrossRef]
53. Yang, Y.; Han, D.; Wu, S.; Lin, H.; Zhang, J.; Zhang, W.; Ye, J. High-performance solar-blind ultraviolet photodetector arrays based on two-inch ε-Ga_2O_3 films for imaging applications. *J. Phys. D Appl. Phys.* **2025**, *58*, 105108. [CrossRef]
54. Chen, Z.; Lu, X.; Tu, Y.; Chen, W.; Zhang, Z.; Cheng, S.; Chen, S.; Luo, H.; He, Z.; Pei, Y.; et al. ε-Ga_2O_3: An emerging wide bandgap piezoelectric semiconductor for application in radio frequency resonators. *Adv. Sci.* **2022**, *9*, 2203927. [CrossRef]
55. Zhang, J.; Liu, N.; Chen, L.; Yang, X.; Guo, H.; Wang, Z.; Yuan, M.Q.; Yan, X.J.; Yang, J.; Li, X.; et al. Ultrawide bandgap diamond/ε-Ga_2O_3 heterojunction Pn diodes with breakdown voltages over 3 kV. *Nano Lett.* **2024**, *25*, 537–544. [CrossRef]
56. Hidouri, T.; Parisini, A.; Dadgostar, S.; Jimenez, J.; Fornari, R. Point defect localization and cathodoluminescence emission in undoped ε-Ga_2O_3. *J. Phys. D Appl. Phys.* **2022**, *55*, 295103. [CrossRef]
57. Huang, H.; Xing, H.; Zhang, W.; Qian, Z.; Wang, L.; Wang, L.; Tang, K.; Huang, J.; Wang, L. Hetero-interface boosted high-performance a-Ga_2O_3 thin-film phototransistors. *Appl. Surf. Sci.* **2025**, *679*, 161179. [CrossRef]
58. Xue, D.; Peng, K.; Chen, C.; Lv, P. Flexible a-Ga_2O_3 solar-blind photodetectors with comprehensive optoelectronic and mechanical properties for imaging sensor arrays and spatial light source detection. *J. Alloys Compd.* **2025**, *1022*, 179836. [CrossRef]
59. Huang, H.; Shen, J.; Liu, X.; Zhong, Y.; Zhang, Z.; Wang, X. Self-assembly of Ni_2P/γ-Ga_2O_3 nanosheets for efficient photocatalytic water splitting hydrogen production. *Dalton Trans.* **2022**, *51*, 17836–17843. [CrossRef]
60. Sun, Y.; Wei, Y.; Li, M.; Zhang, Y.; Li, X.; Fan, L.; Li, Y. Wet chemical synthesis of ultrathin γ-Ga_2O_3 quantum wires enabling far-UVC photodetection with ultrahigh selectivity and sensitivity. *J. Phys. Chem. Lett.* **2024**, *15*, 4301–4310. [CrossRef]
61. Kato, T.; Nishinaka, H.; Shimazoe, K.; Kanegae, K.; Yoshimoto, M. Demonstration of bixbyite-structured δ-Ga_2O_3 thin films using β-Fe_2O_3 buffer layers by mist chemical vapor deposition. *ACS Appl. Electron. Mater.* **2023**, *5*, 1715–1720. [CrossRef]
62. Kato, T.; Shimazoe, K.; Nishinaka, H. Stabilization and Semiconductor Functionality of Metastable δ-Ga_2O_3: Buffer Layer Engineering for Deep UV Photodetection. *ACS Appl. Electron. Mater.* **2025**, *7*, 1432–1438. [CrossRef]
63. Yao, Y.; Gangireddy, R.; Kim, J.; Das, K.K.; Davis, R.F.; Porter, L.M. Electrical behavior of β-Ga_2O_3 Schottky diodes with different Schottky metals. *J. Vac. Sci. Technol. B* **2017**, *35*, 03D113. [CrossRef]
64. Zhang, L.Q.; Miao, W.Q.; Wu, X.L.; Ding, J.Y.; Qin, S.Y.; Liu, J.J.; Tian, Y.T.; Wu, Z.Y.; Zhang, Y.; Xing, Q.; et al. Recent progress in source/drain ohmic contact with β-Ga_2O_3. *Inorganics* **2023**, *11*, 397. [CrossRef]
65. Xue, H.; He, Q.; Jian, G.; Long, S.; Pang, T.; Liu, M. An overview of the ultrawide bandgap Ga_2O_3 semiconductor-based Schottky barrier diode for power electronics application. *Nanoscale Res. Lett.* **2018**, *13*, 290. [CrossRef]
66. Fang, P.; Rao, C.; Liao, C.; Chen, S.; Wu, Z.; Lu, X.; Chen, Z.; Wang, G.; Liang, J.; Pei, Y. Effects of microwave plasma treatment on β-Ga_2O_3 Schottky barrier diodes. *Semicond. Sci. Technol.* **2022**, *37*, 115007. [CrossRef]
67. Ahn, S.; Ren, F.; Yuan, L.; Pearton, S.J.; Kuramata, A. Temperature-dependent characteristics of Ni/Au and Pt/Au Schottky diodes on β-Ga_2O_3. *ECS J. Solid State Sci. Technol.* **2017**, *6*, 68. [CrossRef]
68. Yang, T.H.; Fu, H.; Chen, H.; Huang, X.; Montes, J.; Baranowski, I.; Fu, K.; Zhao, Y. Temperature-dependent electrical properties of β-Ga_2O_3 Schottky barrier diodes on highly doped single-crystal substrates. *J. Semicond.* **2019**, *40*, 012801. [CrossRef]
69. Lee, M.H.; Peterson, R.L. Interfacial reactions of titanium/gold ohmic contacts with Sn-doped β-Ga_2O_3. *APL Mater.* **2019**, *7*, 022524. [CrossRef]
70. Zhou, H.; Si, M.; Alghamdi, S.; Qiu, G.; Yang, L.; Ye, P.D. High-Performance Depletion/Enhancement-mode β-Ga_2O_3 on Insulator (GOOI) Field-Effect Transistors With Record Drain Currents of 600/450 mA/mm. *IEEE Electron Device Lett.* **2016**, *38*, 103–106. [CrossRef]
71. Li, Z.; Liu, Y.; Zhang, A.; Liu, Q.; Shen, C.; Wu, F.; Xu, C.; Chen, M.; Fu, H.; Zhou, C. Quasi-two-dimensional β-Ga_2O_3 field effect transistors with large drain current density and low contact resistance via controlled formation of interfacial oxygen vacancies. *Nano Res.* **2019**, *12*, 143–148. [CrossRef]
72. Spencer, J.A.; Tadjer, M.J.; Jacobs, A.G.; Mastro, M.A.; Lyons, J.L.; Freitas, J.A.; Gallagher, J.C.; Thieu, Q.T.; Sasaki, K.; Kuramata, A.; et al. Activation of implanted Si, Ge, and Sn donors in high-resistivity halide vapor phase epitaxial β-Ga_2O_3 with high mobility. *Appl. Phys. Lett.* **2022**, *121*, 192102. [CrossRef]
73. Sasaki, K.; Higashiwaki, M.; Kuramata, A.; Masui, T.; Yamakoshi, S. Si-ion implantation doping in β-Ga_2O_3 and its application to fabrication of low-resistance ohmic contacts. *Appl. Phys. Express* **2013**, *6*, 086502. [CrossRef]
74. Bhattacharyya, A.; Roy, S.; Ranga, P.; Shoemaker, D.; Song, Y.; Lundh, J.S.; Choi, S.; Krishnamoorthy, S. 130 mA mm^{-1} β-Ga_2O_3 metal semiconductor field effect transistor with low-temperature metal organic vapor phase epitaxy-regrown ohmic contacts. *Appl. Phys. Express* **2021**, *14*, 076502. [CrossRef]

75. Alema, F.; Peterson, C.; Bhattacharyya, A.; Roy, S.; Krishnamoorthy, S.; Osinsky, A. Low resistance ohmic contact on epitaxial MOVPE grown β-Ga_2O_3 and β-$(Al_xGa_{1-x})_2O_3$ films. *IEEE Electron Device Lett.* **2022**, *43*, 1649–1652. [CrossRef]
76. Oshima, T.; Wakabayashi, R.; Hattori, M.; Hashiguchi, A.; Kawano, N.; Sasaki, K.; Masui, T.; Kuramata, A.; Yamakoshi, S.; Yoshimatsu, K.; et al. Formation of indium-tin oxide ohmic contacts for β-Ga_2O_3. *Jpn. J. Appl. Phys.* **2016**, *55*, 1202B7. [CrossRef]
77. Carey, P.H.; Yang, J.; Ren, F.; Hays, D.C.; Pearton, S.J.; Jang, S.; Kuramata, A.; Kravchenko, I.I. Ohmic contacts on n-type β-Ga_2O_3 using AZO/Ti/Au. *AIP Adv.* **2017**, *7*, 095313. [CrossRef]
78. Yao, Y.; Davis, R.F.; Porter, L.M. Investigation of different metals as ohmic contacts to β-Ga_2O_3: Comparison and analysis of electrical behavior, morphology, and other physical properties. *J. Electron. Mater.* **2017**, *46*, 2053–2060. [CrossRef]
79. Higashiwaki, M.; Sasaki, K.; Kuramata, A.; Masui, T.; Yamakoshi, S. Gallium oxide (Ga_2O_3 metal-semiconductor field-effect transistors on single-crystal β-Ga_2O_3 (010) substrates. *Appl. Phys. Lett.* **2012**, *100*, 013504. [CrossRef]
80. Qi, X.; Shen, Y.; Zuo, Y.; Gu, L.; Zhang, Q.C.; Ma, H.P. Low Resistance Ohmic Contact on (100) β-Ga2O3 Substrate with Laser Annealing Using Ti/Au. In Proceedings of the 2024 21st China International Forum on Solid State Lighting & 2024 10th International Forum on Wide Bandgap Semiconductors (SSLCHINA: IFWS), Suzhou, China, 18–21 November 2024; pp. 365–368.
81. Farzana, E.; Zhang, Z.; Paul, P.K.; Arehart, A.R.; Ringel, S.A. Influence of metal choice on (010) β-Ga_2O_3 Schottky diode properties. *Appl. Phys. Lett.* **2017**, *110*, 202102. [CrossRef]
82. Jiang, K.; Lyle, L.A.M.; Favela, E.; Moody, D.; Lin, T.; Das, K.K.; Popp, A.; Galazka, Z.; Wagner, G.; Porter, L.M. Electrical properties of (100) β-Ga_2O_3 Schottky diodes with four different metals. *ECS Trans.* **2017**, *92*, 71. [CrossRef]
83. Bardeen, J. Surface states and rectification at a metal semi-conductor contact. *Phys. Rev.* **1947**, *71*, 717–727. [CrossRef]
84. Lingaparthi, R.; Thieu, Q.T.; Sasaki, K.; Takatsuka, A.; Otsuka, F.; Yamakoshi, S.; Kuramata, A. Effects of Oxygen Annealing of β-Ga_2O_3 Epilayers on the Properties of Vertical Schottky Barrier Diodes. ECS J. *Solid State Sci. Technol.* **2020**, *9*, 024004. [CrossRef]
85. Chen, H.; Wang, H.; Wang, C.; Sheng, K. Low Specific On-Resistance and Low Leakage Current β-Ga_2O_3 (001) Schottky Barrier Diode through Contact Pre-Treatment. In Proceedings of the 34th IEEE International Symposium on Power Semiconductor Devices and ICs (ISPSD), Vancouver, BC, Canada, 22–25 May 2022; pp. 145–148.
86. Deng, Y.; Chen, D.; Li, T.; Zhu, M.; Xu, X.; Zhang, H.; Lu, X. Surface quality improvement mechanism of ICP etching for Ga_2O_3 Schottky barrier diode. *Micro Nanostructures* **2025**, *199*, 208073. [CrossRef]
87. Chatterjee, B.; Jayawardena, A.; Heller, E.; Snyder, D.W.; Dhar, S.; Choi, S. Thermal characterization of gallium oxide Schottky barrier diodes. *Rev. Sci. Instrum.* **2018**, *89*, 114903. [CrossRef]
88. Du, L.; Xin, Q.; Xu, M.; Liu, Y.; Liang, G.; Mu, W.; Jia, Z.; Wang, X.; Xin, G.; Tao, X.T.; et al. Achieving high performance Ga_2O_3 diodes by adjusting chemical composition of tin oxide Schottky electrode. *Semicond. Sci. Technol.* **2019**, *34*, 075001. [CrossRef]
89. Taube, A.; Borysiewicz, M.A.; Sadowski, O.; Wójcicka, A.; Tarenko, J.; Piskorski, K.; Wzorek, M. Investigation of amorphous (Ir,Ru)-Si and (Ir,Ru)-Si-O Schottky contacts to (001) β-Ga_2O_3. Mater. *Sci. Semicond. Process.* **2023**, *154*, 107218. [CrossRef]
90. Farzana, E.; Roy, S.; Hendricks, N.S.; Krishnamoorthy, S.; Speck, J.S. Vertical PtO_x/Pt/β-Ga_2O_3 Schottky diodes with high permittivity dielectric field plate for low leakage and high breakdown voltage. *Appl. Phys. Lett.* **2023**, *123*, 192102. [CrossRef]
91. Dela Cruz, Z.; Hou, C.; Martinez-Gazoni, R.F.; Reeves, R.J.; Allen, M.W. Performance of in situ oxidized platinum/iridium alloy Schottky contacts on (001), (201), and (010) β-Ga_2O_3. *Appl. Phys. Lett.* **2022**, *120*, 083503. [CrossRef]
92. Hou, C.; Makin, R.A.; York, K.R.; Durbin, S.M.; Scott, J.I.; Gazoni, R.M.; Reeves, R.J.; Allen, M.W. High-temperature (350 °C) oxidized iridium Schottky contacts on β-Ga_2O_3. *Appl. Phys. Lett.* **2019**, *114*, 233503. [CrossRef]
93. Watson, J.; Castro, G. A review of high-temperature electronics technology and applications. *J. Mater. Sci. Mater. Electron.* **2015**, *26*, 9226–9235. [CrossRef]
94. Guo, X.; Xun, Q.; Li, Z.; Du, S. Silicon carbide converters and MEMS devices for high-temperature power electronics: A critical review. *Micromachines* **2019**, *10*, 406. [CrossRef]
95. Heinselman, K.; Walker, P.; Norman, A.; Parilla, P.; Ginley, D.; Zakutayev, A. Performance and reliability of β-Ga_2O_3 Schottky barrier diodes at high temperature. *J. Vac. Sci. Technol. A* **2021**, *39*, 040402. [CrossRef]
96. Hou, C.; Gazoni, R.M.; Reeves, R.J.; Allen, M.W. Dramatic Improvement in the Rectifying Properties of Pd Schottky Contacts on β-Ga_2O_3 During Their High-Temperature Operation. *IEEE Trans. Electron Devices* **2021**, *68*, 1791–1797. [CrossRef]
97. Sohel, S.H.; Kotecha, R.; Khan, I.S.; Heinselman, K.N.; Narumanchi, S.; Tellekamp, M.B.; Zakutayev, A. Gallium oxide heterojunction diodes for 400 °C high-temperature applications. *Phys. Status Solidi A* **2023**, *220*, 2300535. [CrossRef]
98. Al-Mamun, N.S.; Li, J.S.; Haque, A.; Wolfe, D.E.; Ren, F.; Pearton, S. High temperature operation and failure of Ga_2O_3 Schottky barrier diodes: An in situ TEM study. *APL Electron. Devices* **2025**, *1*, 016103. [CrossRef]
99. Wang, A.-F.; Ma, H.-P.; Huang, Q.-M.; Gu, L.; Shen, Y.; Ding, C.; Liu, Y.-C.; Xu, K.; Zhucheng, L.; Zhang, L.; et al. Band alignment, thermal transport property, and electrical performance of high-quality β-Ga_2O_3/AlN schottky barrier diode grown via MOCVD. *ACS Appl. Mater. Interfaces* **2025**, *17*, 27517–27529. [CrossRef]
100. Qu, Z.; Xie, Y.; Zhao, T.; Xu, W.; He, Y.; Xu, Y.; Sun, H.; You, T.; Han, G.; Hao, Y.; et al. Extremely low thermal resistance of β-Ga_2O_3 MOSFETs by co-integrated design of substrate engineering and device packaging. *ACS Appl. Mater. Interfaces* **2024**, *16*, 57816–57823. [CrossRef]

101. Peterson, C.; Alema, F.; Bhattacharyya, A.; Ling, Z.; Roy, S.; Osinsky, A.; Krishnamoorthy, S. Kilovolt-class β-Ga_2O_3 MOSFETs on 1-in. bulk substrates. *Appl. Phys. Lett.* **2024**, *124*, 082104. [CrossRef]
102. Su, C.; Zhou, H.; Zhang, K.; Wang, C.; Sun, S.; Gong, H.; Ye, J.; Liu, Z.; Dang, K.; Hu, Z.; et al. Low turn-on voltage and 2.3 kV β-Ga_2O_3 heterojunction barrier Schottky diodes with Mo anode. *Appl. Phys. Lett.* **2024**, *124*, 173506. [CrossRef]
103. Gao, J.; Li, Y.; Lin, W.; Yang, Z.; Gong, M.; Huang, M.; Ma, Y. Enhanced Performance of Vertical β-Ga_2O_3 Schottky Barrier Diodes Through 212-MeV Low-Fluence Ge Ion Irradiation. *IEEE Trans. Electron Devices* **2024**, *71*, 7366–7371. [CrossRef]
104. Hong, Z.; Zhang, C.; Lin, J.; Dai, J.; Zhang, J.; Huang, H.; Yang, W. Low Turn-On Voltage and Reverse Leakage Current β-Ga_2O_3 MIS Schottky Barrier Diodes With an AlN Interfacial Layer. *IEEE Trans. Electron Devices* **2024**, *71*, 6934–6941. [CrossRef]
105. Su, C.; Zhou, H.; Hu, Z.; Wang, C.; Hao, Y.; Zhang, J. 1.96 kV p-Cr_2O_3/β-Ga_2O_3 heterojunction diodes with an ideality factor of 1.07. *Appl. Phys. Lett.* **2025**, *126*, 132104.
106. Feng, Y.; Zhou, H.; Alghamdi, S.; Wasly, S.; Hao, Y.; Zhang, J. 1.5 kV β-Ga_2O_3 vertical Schottky diodes with 58 A surge current and off-state stressing study. *Appl. Phys. Lett.* **2025**, *126*, 182101. [CrossRef]
107. Tetzner, K.; Halhoul, H.; Cuallo, M.D.; Hilt, O. 4 A/300 V switching of lateral β-Ga_2O_3 MOSFET devices. *IEEE Electron Device Lett.* **2025**, preprint. [CrossRef]
108. Ma, H.; Yang, D.; Zhu, M.; Xu, X.; Li, T.; Zhang, H.; Lu, X. Theoretical Analysis of Vertical β-Ga_2O_3 Schottky Barrier Diodes With p-NiO Field Limiting Rings for High P-FOM Performance. *IEEE J. Electron Devices Soc.* **2025**, preprint. [CrossRef]
109. Cai, Y.; Feng, Z.; Wang, Z.; Song, X.; Hu, Z.; Tian, X.; Zhang, C.; Liu, Z.; Feng, Q.; Zhou, H.; et al. Demonstration of the normally off β-Ga_2O_3 MOSFET with high threshold voltage and high current density. *Appl. Phys. Lett.* **2023**, *123*, 193501.
110. Chen, H.; Li, Z.; Zhang, Z.; Liu, D.; Zeng, L.; Yan, Y.; Chen, D.; Feng, Q.; Zhang, J.; Hao, Y.; et al. Review of β-Ga_2O_3 solar-blind ultraviolet photodetector: Growth, device, and application. *Semicond. Sci. Technol.* **2024**, *39*, 063001.
111. Zhang, Z.; Liu, D.; Yan, Y.; Zeng, L.; Chen, H.; Song, Q.; Chen, D.; Zhu, C.; Zhang, C.; Zhang, Y.; et al. β-Ga_2O_3 Photodetectors with High-Performance Enhanced by Field Control via p-Type NiO Interlayer. *J. Alloys Compd.* **2025**, *1031*, 181097.
112. Xu, Y.; Cheng, Y.; Li, Z.; Chen, D.; Xu, S.; Feng, Q.; Zhu, W.; Zhang, Y.; Zhang, J.; Zhang, C.; et al. Ultra high-performance solar-blind photodetectors based on high quality heteroepitaxial single crystalline β-Ga_2O_3 film grown by vacuum free, low-cost mist chemical vapor deposition. *Adv. Mater. Technol.* **2021**, *6*, 2001296. [CrossRef]
113. Sun, Q.; Wei, J.; Han, W.; Sang, K.; Wu, D.; Zeng, L.; Pei, K.; Wang, B.; Shen, L.; Yuan, J.; et al. Solar-blind β-Ga_2O_3 photodetectors with high detectivity via semimetal Bi contacts. *Surf. Interfaces* **2025**, *60*, 106052. [CrossRef]
114. Chang, Q.; Hou, B.; Yang, L.; Jia, M.; Zhu, Y.; Wu, M.; Zhang, M.; Zhu, Q.; Lu, H.; Xu, J.; et al. 3 kV fully vertical β-Ga_2O_3 junction termination extension Schottky barrier diode with sputtered p-GaN. *Appl. Phys. Lett.* **2025**, *126*, 062102. [CrossRef]
115. Wang, C.; Sun, S.; Su, C.; Zhou, H.; Zhang, J.; Hao, Y. Breakdown voltage over 10 kV β-Ga_2O_3 heterojunction FETs with RESURF structure. *Sci. China Inf. Sci.* **2025**, *68*, 169401. [CrossRef]
116. Pearton, S.J.; Ren, F.; Tadjer, M.; Kim, J. Perspective: Ga_2O_3 for ultra-high power rectifiers and MOSFETS. *J. Appl. Phys.* **2018**, *124*, 220901.
117. Yang, J.; Ren, F.; Tadjer, M.; Pearton, S.J.; Kuramata, A. 2300V reverse breakdown voltage Ga_2O_3 Schottky rectifiers. *ECS J. Solid State Sci. Technol.* **2018**, *7*, Q92.
118. Gao, X.; Xie, T.; Wu, J.; Fu, J.; Gao, X.; Xie, M.; Zhao, H.; Wang, Y.; Shi, Z. Ultraviolet communication system utilizing effective performance β-Ga_2O_3 photodetector. *Appl. Phys. Lett.* **2024**, *125*, 172103.
119. Li, R.; Wang, W.; Li, Y.; Gao, S.; Yue, W.; Shen, G. Multi-modulated optoelectronic memristor based on Ga_2O_3/MoS_2 heterojunction for bionic synapses and artificial visual system. *Nano Energy* **2023**, *111*, 108398.
120. Sasaki, K.; Higashiwaki, M.; Kuramata, A.; Masui, T.; Yamakoshi, S. β-Ga_2O_3 Schottky Barrier Diodes Fabricated by Using Single-Crystal β-Ga_2O_3 (010) Substrates. *IEEE Electron Device Lett.* **2013**, *34*, 493–495. [CrossRef]
121. Higashiwaki, M.; Sasaki, K.; Goto, K.; Nomura, K.; Thieu, Q.T.; Togashi, R.; Murakami, H.; Kumagai, Y.; Monemar, B.; Koukitu, A.; et al. Ga_2O_3 Schottky barrier diodes with n^--Ga_2O_3 drift layers grown by HVPE. In Proceedings of the 2015 73rd Annual Device Research Conference (DRC), Columbus, OH, USA, 21–24 June 2015; pp. 29–30.
122. Oda, M.; Tokuda, R.; Kambara, H.; Tanikawa, T.; Sasaki, T.; Hitora, T. Schottky barrier diodes of corundum-structured gallium oxide showing on-resistance of 0.1 $m\Omega \cdot cm^2$ grown by MIST EPITAXY. *Appl. Phys. Express* **2016**, *9*, 021101. [CrossRef]
123. Yang, J.; Ren, F.; Pearton, S.J.; Kuramata, A. Vertical Geometry, Vertical geometry, 2-A forward current Ga_2O_3 Schottky rectifiers on bulk Ga_2O_3 substrates. *IEEE Trans. Electron Devices* **2018**, *65*, 2790–2796. [CrossRef]
124. Yang, J.; Ahn, S.; Ren, F.; Pearton, S.J.; Jang, S.; Kuramata, A. High breakdown voltage (−201) β-Ga_2O_3 Schottky rectifiers. *IEEE Electron Device Lett.* **2017**, *38*, 906–909.
125. Fu, H.; Chen, H.; Huang, X.; Baranowski, I.; Montes, J.; Yang, T.-H.; Zhao, Y. A Comparative Study on the Electrical Properties of Vertical (−201) and (010) β-Ga_2O_3 Schottky Barrier Diodes on EFG Single-Crystal Substrates. *IEEE Trans. Electron Devices* **2018**, *65*, 3507–3513. [CrossRef]
126. He, Q.; Hao, W.; Zhou, X.; Li, Y.; Zhou, K.; Chen, C.; Xiong, W.; Jian, G.; Xu, G.; Zhao, X.; et al. Over 1 GW/cm^2 vertical Ga_2O_3 Schottky barrier diodes without edge termination. *IEEE Electron Device Lett.* **2021**, *43*, 264–267. [CrossRef]

127. Chiang, C.-C.; Xia, X.; Li, J.-S.; Ren, F.; Pearton, S.J. Selective wet and dry etching of NiO over β-Ga_2O_3. *ECS J. Solid State Sci. Technol.* **2022**, *11*, 104001. [CrossRef]
128. Yang, J.; Sparks, Z.; Ren, F.; Pearton, S.J.; Tadjer, M. Effect of surface treatments on electrical properties of β-Ga_2O_3. *J. Vac. Sci. Technol. B* **2018**, *36*, 061201. [CrossRef]
129. Janardhanam, V.; Kim, J.-H.; Jyothi, I.; Jung, H.-H.; Kim, S.-J.; Shim, K.-H.; Choi, C.-J. Enhancement of device performance in β-Ga_2O_3 Schottky barrier diodes with tetramethylammonium hydroxide treatment. *Colloids Surf. A Physicochem. Eng. Asp.* **2024**, *693*, 134079. [CrossRef]
130. Yu, C.; Hu, H.; Wang, Y.; Jia, X.; Huang, S.; Luo, Z.; Li, B.; Fang, C.; Li, X.; Liu, Y.; et al. Enhancing β-Ga_2O_3 Schottky Barrier Diodes' Performance Through Low-Temperature Post-Annealing: Achieving Optimal Forward Current-Voltage Characteristics. *IEEE Trans. Electron Devices* **2024**, *71*, 5552–5558. [CrossRef]
131. Liu, H.; Han, S.; Lu, X.; Wang, Y.; Dun, S.; Han, T.; Lv, Y.; Feng, Z. Demonstration of Vertical Ga_2O_3 Schottky Barrier Diodes Directly on Heavily Doped Single-Crystal Substrate Using Thermal Oxidation Technology. *Eur. Phys. J. Spec. Top.* **2025**, *234*, 283–290. [CrossRef]
132. Yu, H.; Wang, J.; Zhang, J.; Liang, S.; Shen, Z.J. Theoretical analysis and experimental characterization of 1.2-kV 4H-SiC planar split-gate MOSFET with source field plate. *IEEE Trans. Electron Devices* **2023**, *71*, 1508–1512. [CrossRef]
133. Tarplee, M.C.; Madangarli, V.P.; Zhang, Q.; Sudarshan, T.S. Design rules for field plate edge termination in SiC Schottky diodes. *IEEE Trans. Electron Devices* **2001**, *48*, 2659–2664. [CrossRef]
134. Wu, Y.F.; Saxler, A.; Moore, M.; Smith, R.P.; Sheppard, S.; Chavarkar, P.M.; Wisleder, T.; Mishra, U.K.; Parikh, P. 30-W/mm GaN HEMTs by field plate optimization. *IEEE Electron Device Lett.* **2004**, *25*, 117–119. [CrossRef]
135. Lei, Y.; Shi, H.; Lu, H.; Chen, D.; Zhang, R.; Zheng, Y. Field plate engineering for GaN-based Schottky barrier diodes. *J. Semicond.* **2013**, *34*, 054007. [CrossRef]
136. Konishi, K.; Goto, K.; Murakami, H.; Kumagai, Y.; Kuramata, A.; Yamakoshi, S.; Higashiwaki, M. 1-kV vertical Ga_2O_3 field-plated Schottky barrier diodes. *Appl. Phys. Lett.* **2017**, *110*, 103506. [CrossRef]
137. Roy, S.; Bhattacharyya, A.; Ranga, P.; Splawn, H.; Leach, J.; Krishnamoorthy, S. High-k oxide field-plated vertical (001) β-Ga_2O_3 Schottky barrier diode with Baliga's figure of merit over 1 GW/cm^2. *IEEE Electron Device Lett.* **2021**, *42*, 1140–1143. [CrossRef]
138. Roy, S.; Bhattacharyya, A.; Peterson, C.; Krishnamoorthy, S. 2.1 kV (001)-β-Ga_2O_3 vertical Schottky barrier diode with high-k oxide field plate. *Appl. Phys. Lett.* **2023**, *122*, 152101. [CrossRef]
139. Hu, Z.; Li, J.; Zhao, C.; Feng, Z.; Tian, X.; Zhang, Y.; Zhang, Y.; Ning, J.; Zhou, H.; Zhang, C.; et al. Design and fabrication of vertical metal/TiO_2/β-Ga_2O_3 dielectric heterojunction diode with reverse blocking voltage of 1010 V. *IEEE Trans. Electron Devices* **2020**, *67*, 5628–5632. [CrossRef]
140. Farzana, E.; Bhattacharyya, A.; Hendricks, N.S.; Itoh, T.; Krishnamoorthy, S.; Speck, J.S. Oxidized metal Schottky contact with high-κ dielectric field plate for low-loss high-power vertical β-Ga_2O_3 Schottky diodes. *APL Mater.* **2022**, *10*, 111104. [CrossRef]
141. Carey, P.H.; Yang, J.; Ren, F.; Sharma, R.; Law, M.; Pearton, S.J. Comparison of dual-stack dielectric field plates on β-Ga_2O_3 Schottky rectifiers. *ECS J. Solid State Sci. Technol.* **2019**, *8*, Q3221. [CrossRef]
142. Yang, J.; Ren, F.; Chen, Y.T.; Liao, Y.T.; Chang, C.W.; Lin, J.; Tadjer, M.J.; Pearton, S.J.; Kuramata, A. Dynamic Switching Characteristics of 1 A Forward Current β-Ga_2O_3 Rectifiers. *IEEE J. Electron Devices Soc.* **2018**, *7*, 57–61. [CrossRef]
143. Yuda, Y.; Ebihara, K.; Nanjo, T.; Furuhashi, M.; Watahiki, T.; Nishikawa, K. A simulation study of vertical Ga_2O_3 Schottky barrier diodes using field plate termination. *Jpn. J. Appl. Phys.* **2024**, *63*, 02SP66. [CrossRef]
144. Lee, H.-K.; Janardhanam, V.; Mun, J.-K.; Jang, T.-H.; Shim, K.-H.; Yun, H.J.; Won, J.; Choi, C.-J. Enhancement of device performance in vertical Au/Ni/β-Ga_2O_3 Schottky barrier diodes using regularly aligned inner field plates. *Mater. Sci. Semicond. Process.* **2025**, *191*, 109371. [CrossRef]
145. Gilankar, A.; Islam, A.E.; McCartney, M.R.; Katta, A.; Das, N.; Smith, D.J.; Kalarickal, N.K. Three-step field-plated β-Ga_2O_3 Schottky barrier diodes and heterojunction diodes with sub-1 V turn-on and kilovolt-class breakdown. *Appl. Phys. Express* **2024**, *17*, 046501.
146. Bae, J.; Kim, H.W.; Kang, I.H.; Kim, J. Dual-field plated β-Ga_2O_3 nano-FETs with an off-state breakdown voltage exceeding 400 V. *J. Mater. Chem. C* **2020**, *8*, 2687–2692. [CrossRef]
147. Han, S.; Wang, Y.; Lv, Y.; Liu, H.; Han, T.; Dun, S.; Feng, Z. High-performance Ga_2O_3 Schottky Barrier Diode with a Self-aligned Shallow Groove and Dual Field-plate. In Proceedings of the 8th International Conference on Integrated Circuits and Microsystems (ICICM), Nanjing, China, 20–23 October 2023; pp. 86–91.
148. Guo, W.; Jian, G.; Hao, W.; Wu, F.; Zhou, K.; Du, J.; Zhou, X.; He, Q.; Yu, Z.; Zhao, X.; et al. β-Ga_2O_3 field plate schottky barrier diode with superb reverse recovery for high-efficiency DC-DC converter. *IEEE J. Electron Devices Soc.* **2022**, *10*, 933–941. [CrossRef]
149. Allen, N.; Xiao, M.; Yan, X.; Sasaki, K.; Tadjer, M.J.; Ma, J.; Zhang, R.; Wang, H.; Zhang, Y. Vertical Ga_2O_3 Schottky barrier diodes with small-angle beveled field plates: A Baliga's figure-of-merit of 0.6 GW/cm^2. *IEEE Electron Device Lett.* **2019**, *40*, 1399–1402. [CrossRef]

150. Liu, D.; Huang, Y.; Zhang, Z.; Chen, D.; Feng, Q.; You, H.; Zhang, J.; Zhang, C.; Hao, Y. Enhancing breakdown voltage of a Ga_2O_3 Schottky barrier diode with small-angle beveled and high-k oxide field plate. *ECS J. Solid State Sci. Technol.* **2021**, *10*, 125001. [CrossRef]
151. Chen, H.; Wang, H.; Sheng, K. Vertical β-Ga_2O_3 Schottky barrier diodes with field plate assisted negative beveled termination and positive beveled termination. *IEEE Electron Device Lett.* **2022**, *44*, 21–24. [CrossRef]
152. Joishi, C.; Rafique, S.; Xia, Z.; Han, L.; Krishnamoorthy, S.; Zhang, Y.; Lodha, S.; Zhao, H.; Rajan, S. Low-pressure CVD-grown β-Ga_2O_3 bevel-field-plated Schottky barrier diodes. *Appl. Phys. Express* **2018**, *11*, 031101. [CrossRef]
153. Sun, N.; Gong, H.H.; Hu, T.C.; Zhou, F.; Wang, Z.P.; Yu, X.X.; Ren, F.-F.; Gu, S.L.; Lu, H.; Zhang, R.; et al. Fast switching Ga_2O_3 Schottky barrier power diode with beveled-mesa and $BaTiO_3$ field plate edge termination. *Appl. Phys. Lett.* **2024**, *125*, 172104. [CrossRef]
154. Wu, F.; Wang, Y.; Jian, G.; Xu, G.; Zhou, X.; Guo, W.; Du, J.; Liu, Q.; Dun, S.; Yu, Z.; et al. Superior performance β-Ga_2O_3 junction barrier Schottky diodes implementing p-NiO heterojunction and beveled field plate for hybrid Cockcroft-Walton voltage multiplier. *IEEE Trans. Electron Devices* **2023**, *70*, 1199–1205. [CrossRef]
155. Wang, H.; Jiang, L.-L.; Lin, X.-P.; Lei, S.-Q.; Yu, H.-Y. A simulation study of field plate termination in Ga_2O_3 Schottky barrier diodes. *Chin. Phys. B* **2018**, *27*, 127302. [CrossRef]
156. Zhou, H.; Yan, Q.; Zhang, J.; Lv, Y.; Liu, Z.; Zhang, Y.; Dang, K.; Dong, P.; Feng, Z.; Feng, Q.; et al. High-Performance Vertical β-Ga_2O_3 Schottky Barrier Diode with Implanted Edge Termination. *IEEE Electron Device Lett.* **2019**, *40*, 1788–1791. [CrossRef]
157. Zhang, Y.; Zhang, J.; Feng, Z.; Hu, Z.; Chen, J.; Dang, K.; Yan, Q.; Dong, P.; Zhou, H.; Hao, Y. Impact of implanted edge termination on vertical β-Ga_2O_3 Schottky barrier diodes under OFF-state stressing. *IEEE Trans. Electron Devices* **2020**, *67*, 3948–3953. [CrossRef]
158. Gao, Y.; Li, A.; Feng, Q.; Hu, Z.; Feng, Z.; Zhang, K.; Lu, X.; Zhang, C.; Zhou, H.; Mu, W.; et al. High-voltage β-Ga_2O_3 Schottky diode with argon-implanted edge termination. *Nanoscale Res. Lett.* **2019**, *14*, 8. [CrossRef]
159. Hu, Z.; Lv, Y.; Zhao, C.; Feng, Q.; Feng, Z.; Dang, K.; Tian, X.; Zhang, Y.; Ning, J.; Zhou, H.; et al. Beveled Fluoride Plasma Treatment for Vertical β-Ga_2O_3 Schottky Barrier Diode with High Reverse Blocking Voltage and Low Turn-On Voltage. *IEEE Electron Device Lett.* **2020**, *41*, 441–444. [CrossRef]
160. Luo, X.; Hao, L.; Wei, Y.; Dai, K.; Peng, X.; Jiang, Z.; Wu, Y. High breakdown voltage β-Ga_2O_3 Schottky barrier diode with fluorine-implanted termination. *Microelectron. J.* **2024**, *150*, 106269. [CrossRef]
161. Lin, C.H.; Yuda, Y.; Wong, M.H.; Sato, M.; Takekawa, N.; Konishi, K.; Watahiki, T.; Yamamuka, M.; Murakami, H.; Kumagai, Y.; et al. Vertical Ga_2O_3 Schottky barrier diodes with guard ring formed by nitrogen-ion implantation. *IEEE Electron Device Lett.* **2019**, *40*, 1487–1490. [CrossRef]
162. Sharma, R.; Patrick, E.E.; Law, M.E.; Ren, F.; Pearton, S.J. Optimization of edge termination techniques for β-Ga_2O_3 Schottky rectifiers. *ECS J. Solid State Sci. Technol.* **2019**, *8*, Q234. [CrossRef]
163. Wang, B.; Feng, C.; Jiang, L.; Xiao, H.; Li, W.; Wang, X. Optimization of Finite-Zone Implanted Edge Termination for β-Ga_2O_3 SBD. *ECS J. Solid State Sci. Technol.* **2022**, *11*, 055009. [CrossRef]
164. Lu, X.; Zhang, X.; Jiang, H.; Zou, X.; Lau, K.M. Vertical Schottky barrier diodes based on a bulk β-Ga_2O_3 substrate with high switching performance. In Proceedings of the 2019 Compound Semiconductor Week (CSW), Nara, Japan, 19–23 May 2019; p. 1.
165. Wen, J.; Hao, W.; Han, Z.; Wu, F.; Li, Q.; Liu, J.; Liu, Q.; Zhou, X.; Xu, G.; Yang, S.; et al. Vertical β-Ga_2O_3 Power Diodes: From Interface Engineering to Edge Termination. *IEEE Trans. Electron Devices* **2024**, *71*, 1606–1617. [CrossRef]
166. Wang, Y.; Lv, Y.; Long, S.; Zhou, X.; Song, X.; Liang, S.; Han, T.; Tan, X.; Feng, Z.; Cai, S.; et al. High-Voltage (201) β-Ga_2O_3 Vertical Schottky Barrier Diode with Thermally-Oxidized Termination. *IEEE Electron Device Lett.* **2019**, *41*, 131–134. [CrossRef]
167. He, Q.; Zhou, X.; Li, Q.; Hao, W.; Liu, Q.; Han, Z.; Zhou, K.; Chen, C.; Peng, J.; Xu, G.; et al. Selective high-resistance zones formed by oxygen annealing for-Ga_2O_3 Schottky diode applications. *IEEE Electron Device Lett.* **2022**, *43*, 1933–1936.
168. Oshima, T.; Kaminaga, K.; Mukai, A.; Sasaki, K.; Masui, T.; Kuramata, A.; Yamakoshi, S.; Fujita, S.; Ohtomo, A. Formation of semi-insulating layers on semiconducting β-Ga_2O_3 single crystals by thermal oxidation. *Jpn. J. Appl. Phys.* **2013**, *52*, 051101. [CrossRef]
169. Jesenovec, J.; Weber, M.H.; Pansegrau, C.; McCluskey, M.D.; Lynn, K.G.; McCloy, J.S. Gallium vacancy formation in oxygen annealed β-Ga_2O_3. *J. Appl. Phys.* **2021**, *129*, 245701. [CrossRef]
170. Sun, R.; Ooi, Y.K.; Ranga, P.; Bhattacharyya, A.; Krishnamoorthy, S.; Scarpulla, M.A. Oxygen annealing induced changes in defects within β-Ga_2O_3 epitaxial films measured using photoluminescence. *J. Phys. D Appl. Phys.* **2021**, *54*, 174004.
171. Tadjer, M.J.; Freitas, J.A.; Culbertson, J.C.; Weber, M.H.; Glaser, E.R.; Mock, A.L.; Mahadik, N.A.; Schmieder, K.; Jackson, E.; Gallagher, J.C.; et al. Structural and electronic properties of Si-and Sn-doped (−201) β-Ga_2O_3 annealed in nitrogen and oxygen atmospheres. *J. Phys. D Appl. Phys.* **2020**, *53*, 504002. [CrossRef]
172. Dong, P.; Zhang, J.; Yan, Q.; Liu, Z.; Ma, P.; Zhou, H.; Hao, Y. 6 kV/3.4 m$\Omega \cdot cm^2$ vertical β-Ga_2O_3 Schottky barrier diode with $BV^2/R_{on,sp}$ performance exceeding 1-D unipolar limit of GaN and SiC. *IEEE Electron Device Lett.* **2022**, *43*, 765–768. [CrossRef]
173. Sasaki, K.; Wakimoto, D.; Thieu, Q.T.; Koishikawa, Y.; Kuramata, A.; Higashiwaki, M.; Yamakoshi, S. First demonstration of Ga_2O_3 trench MOS-type Schottky barrier diodes. *IEEE Electron Device Lett.* **2017**, *38*, 783–785.

174. Li, W.; Nomoto, K.; Hu, Z.; Tanen, N.; Sasaki, K.; Kuramata, A.; Jena, D.; Xing, H.G. 1.5 kV vertical Ga_2O_3 trench-MIS Schottky barrier diodes. In Proceedings of the 2018 76th Device Research Conference (DRC), Santa Barbara, CA, USA, 24–27 June 2018; pp. 1–2.
175. Li, W.; Hu, Z.; Nomoto, K.; Zhang, Z.; Hsu, J.Y.; Thieu, Q.T.; Sasaki, K.; Kuramata, A.; Jena, D.; Xing, H.G. 1230 V β-Ga_2O_3 trench Schottky barrier diodes with an ultra-low leakage current of <1 μA/cm^2. *Appl. Phys. Lett.* **2018**, *113*, 202101.
176. Li, W.; Hu, Z.; Nomoto, K.; Jinno, R.; Zhang, Z.; Tu, T.Q.; Sasaki, K.; Kuramata, A.; Jena, D.; Xing, H.G. 2.44 kV Ga_2O_3 vertical trench Schottky barrier diodes with very low reverse leakage current. In Proceedings of the 2018 IEEE International Electron Devices Meeting (IEDM), San Francisco, CA, USA, 1–5 December 2018; pp. 8.5.1–8.5.4.
177. Huang, X.; Liao, F.; Li, L.; Liang, X.; Liu, Q.; Zhang, C.; Hu, X. 3.4 kV breakdown voltage Ga_2O_3 trench Schottky diode with optimized trench corner radius. *ECS J. Solid State Sci. Technol.* **2020**, *9*, 045012.
178. Li, W.; Nomoto, K.; Hu, Z.; Jena, D.; Xing, H.G. Field-Plated Ga_2O_3 Trench Schottky Barrier Diodes with a $BV^2/R_{on,sp}$ of up to 0.95 GW/cm^2. *IEEE Electron Device Lett.* **2019**, *41*, 107–110.
179. Yi, B.; Xia, J.; Qiao, Y.; Zhang, Z.; Zhang, B.; Yu, G.; Qian, L.; Cheng, J.; Huang, H.; Kong, M.; et al. 1380 V β-Ga_2O_3 trench MIS-type Schottky barrier diode with ultra-low leakage current. *Jpn. J. Appl. Phys.* **2025**, *64*, 030906. [CrossRef]
180. Kim, H.S.; Bhat, A.K.; Smith, M.D.; Kuball, M. Turn-On Voltage Instability of β-Ga_2O_3 Trench Schottky Barrier Diodes With Different Fin Channel Orientations. *IEEE Trans. Electron Devices* **2024**, *71*, 3609–3613. [CrossRef]
181. Dhara, S.; Dheenan, A.; Rajan, S. Charge recovery by vacuum annealing in β-Ga_2O_3 multi-fin trench Schottky barrier diodes. *APL Electron. Devices* **2025**, *1*, 026122. [CrossRef]
182. Ji, X.Q.; Yue, J.Y.; Wang, J.J.; Zheng, H.C.; Li, S.; Liu, Z.; Shu, L.; Tang, W.H.; Li, P.G. Edge-Field-Suppression for Improved Breakdown and Leakage in Vertical β-Ga_2O_3 Schottky Barrier Diode Through Trench Field Limiting Rings. *IEEE Trans. Electron Devices* **2024**, *71*, 7696–7701. [CrossRef]
183. Li, W.; Nomoto, K.; Hu, Z.; Jena, D.; Xing, H.G. ON-resistance of Ga_2O_3 trench-MOS Schottky barrier diodes: Role of sidewall interface trap. *IEEE Trans. Electron Devices* **2021**, *68*, 2420–2426. [CrossRef]
184. Tang, W.; Zhang, X.; He, T.; Ma, Y.; Feng, B.; Wei, X.; He, G.; Zhang, S.; Huo, X.; Cai, Y.; et al. Temperature-dependent electrical characteristics of β-Ga_2O_3 trench Schottky barrier diodes via self-reactive etching. *J. Phys. D Appl. Phys.* **2021**, *54*, 425104.
185. Dhara, S.; Kalarickal, N.K.; Dheenan, A.; Rahman, S.I.; Joishi, C.; Rajan, S. β-Ga_2O_3 trench Schottky diodes by low-damage Ga-atomic beam etching. *Appl. Phys. Lett.* **2023**, *123*, 023503. [CrossRef]
186. Roy, S.; Kostroun, B.; Liu, Y.; Cooke, J.; Bhattacharyya, A.; Peterson, C.; Sensale-Rodriguez, B.; Krishnamoorthy, S. Low Q_CV_F 20A/1.4 kV β-Ga_2O_3 Vertical Trench High-k RESURF Schottky Barrier Diode with Turn-on Voltage of 0.5 V. *IEEE Electron Device Lett.* **2024**, *45*, 2487–2490. [CrossRef]
187. Li, W.; Nomoto, K.; Hu, Z.; Jena, D.; Xing, H.G. Fin-channel orientation dependence of forward conduction in kV-class Ga_2O_3 trench Schottky barrier diodes. *Appl. Phys. Express* **2019**, *12*, 061007. [CrossRef]
188. Otsuka, F.; Miyamoto, H.; Takatsuka, A.; Kunori, S.; Sasaki, K.; Kuramata, A. Large-size (1.7 × 1.7 mm^2) β-Ga_2O_3 field-plated trench MOS-type Schottky barrier diodes with 1.2 kV breakdown voltage and 10^9 high on/off current ratio. *Appl. Phys. Express* **2021**, *15*, 016501. [CrossRef]
189. Li, W.; Nomoto, K.; Hu, Z.; Jena, D.; Xing, H.G. Guiding principles for trench Schottky barrier diodes based on ultrawide bandgap semiconductors: A case study in Ga_2O_3. *IEEE Trans. Electron Devices* **2020**, *67*, 3938–3947.
190. Dhara, S.; Kalarickal, N.K.; Dheenan, A.; Joishi, C.; Rajan, S. β-Ga_2O_3 Schottky barrier diodes with 4.1 MV/cm field strength by deep plasma etching field-termination. *Appl. Phys. Lett.* **2022**, *121*, 203501.
191. Han, Z.; Jian, G.; Zhou, X.; He, Q.; Hao, W.; Liu, J.; Li, B.; Huang, H.; Li, Q.; Zhao, X.; et al. 2.7 kV low leakage vertical PtO_x/β-Ga_2O_3 Schottky barrier diodes with self-aligned mesa termination. *IEEE Electron Device Lett.* **2023**, *44*, 1680–1683. [CrossRef]
192. Zhang, F.; Feng Zheng, X.; Hong Li, Y.; Jian Yuan, Z.; Zhong Yue, S.; Chen Wang, X.; Long He, Y.; Li Lu, X.; Hua Ma, X.; Hao, Y. Enhancement of positive bevel β-Ga_2O_3 trench MOS barrier Schottky diode by post-etching treatment. *Appl. Surf. Sci.* **2025**, *684*, 161569. [CrossRef]
193. Wan, J.; Wang, H.; Wang, C.; Chen, H.; Zhang, C.; Zhang, L.; Li, Y.; Sheng, K. 2.5 kV/3.78 mΩ·cm^2 low forward voltage vertical β-Ga_2O_3 Schottky rectifier with field plate assisted deep mesa termination. *IEEE Electron Device Lett.* **2024**, *45*, 778–781. [CrossRef]
194. Feng, Z.; Han, S.; Wang, Y.; Guo, H.; Dun, S.; Liu, H.; Han, T.; Lv, Y. 1200-V/10-A Low Thermal Resistance Ga_2O_3 Schottky Barrier Diode with Composite Terminal Structure and Substrate Thinning. *IEEE Trans. Electron Devices* **2025**, *72*, 3738–3743. [CrossRef]
195. Wei, Y.; Luo, X.; Wang, Y.; Peng, X.; Hao, L.; Zhao, K.; Wei, J.; Li, X.; Jiang, Z.; Dun, S.; et al. 600V/7A Large-Size RESURF β-Ga_2O_3 Schottky Barrier Diode with High-Temperature Storage Test. *IEEE Trans. Electron Devices* **2023**, *71*, 1320–1324. [CrossRef]
196. Wu, F.; Han, Z.; Liu, J.; Wang, Y.; Hao, W.; Zhou, X.; Xu, G.; Lv, Y.; Feng, Z.; Long, S. 8.7 A/700 V β-Ga_2O_3 Schottky barrier diode demonstrated by oxygen annealing combined with self-aligned mesa termination. *Appl. Phys. Express* **2024**, *17*, 036504. [CrossRef]
197. Okumura, H.; Tanaka, T. Dry and wet etching for β-Ga_2O_3 Schottky barrier diodes with mesa termination. *Jpn. J. Appl. Phys.* **2019**, *58*, 120902. [CrossRef]

198. Hao, W.; He, Q.; Zhou, K.; Xu, G.; Xiong, W.; Zhou, X.; Jian, G.; Chen, C.; Zhao, X.; Long, S. Low defect density and small I-V curve hysteresis in NiO/β-Ga_2O_3 pn diode with a high PFOM of 0.65 GW/cm^2. *Appl. Phys. Lett.* **2021**, *118*, 043501. [CrossRef]
199. Liu, D.; Zhang, Z.; Chai, W.; Chen, H.; Peng, G.; Zeng, L.; Wang, C.; Chen, D.; Feng, Q.; Zhou, H.; et al. Interface modification-induced high-performance vertical NiO_x/β-Ga_2O_3 heterojunction diodes via O_2 plasma treatment. *Appl. Surf. Sci.* **2025**, *699*, 163147. [CrossRef]
200. Hao, J.G.; Gong, H.H.; Chen, X.H.; Xu, Y.; Ren, F.-F.; Gu, S.L.; Zhang, R.; Zheng, Y.D.; Ye, J.D. In situ heteroepitaxial construction and transport properties of lattice-matched α-Ir_2O_3/α-Ga_2O_3 pn heterojunction. *Appl. Phys. Lett.* **2021**, *118*, 261601. [CrossRef]
201. Kan, S.-I.; Takemoto, S.; Kaneko, K.; Takahashi, I.; Sugimoto, M.; Shinohe, T.; Fujita, S. Electrical properties of α-Ir_2O_3/α-Ga_2O_3 pn heterojunction diode and band alignment of the heterostructure. *Appl. Phys. Lett.* **2018**, *113*, 212104. [CrossRef]
202. Budde, M.; Splith, D.; Mazzolini, P.; Tahraoui, A.; Feldl, J.; Ramsteiner, M.; von Wenckstern, H.; Grundmann, M.; Bierwagen, O. SnO/β-Ga_2O_3 vertical pn heterojunction diodes. *Appl. Phys. Lett.* **2020**, *117*, 252106.
203. Tetzner, K.; Egbo, K.; Klupsch, M.; Unger, R.-S.; Popp, A.; Chou, T.-S.; Anooz, S.B.; Galazka, Z.; Trampert, A.; Bierwagen, O.; et al. SnO/β-Ga_2O_3 heterojunction field-effect transistors and vertical p-n diodes. *Appl. Phys. Lett.* **2022**, *120*, 112110. [CrossRef]
204. Yu, M.; Wang, H.; Wei, W.; Peng, B.; Yuan, L.; Hu, J.; Zhang, Y.; Jia, R. Analysis of electronic structure and properties of Ga_2O_3/$CuAlO_2$ heterojunction. *Appl. Surf. Sci.* **2021**, *568*, 150826. [CrossRef]
205. Prasad, C.V.; Park, J.H.; Min, J.Y.; Song, W.; Labed, M.; Jung, Y.; Kyoung, S.; Kim, S.; Sengouga, N.; Rim, Y.S. Interface engineering of p-type quaternary metal oxide semiconductor interlayer-embedded β-Ga_2O_3 Schottky barrier diode. *Mater. Today Phys.* **2023**, *30*, 100932. [CrossRef]
206. Montes, J.; Yang, C.; Fu, H.; Yang, T.H.; Fu, K.; Chen, H.; Zhou, J.; Huang, X.; Zhao, Y. Demonstration of mechanically exfoliated β-$Ga_2O_{3/}$GaN pn heterojunction. *Appl. Phys. Lett.* **2019**, *114*, 162103. [CrossRef]
207. Liu, Y.; Wang, L.; Zhang, Y.; Dong, X.; Sun, X.; Hao, Z.; Luo, Y.; Sun, C.; Han, Y.; Xiong, B.; et al. Demonstration of n-Ga_2O_3/p-GaN diodes by wet-etching lift-off and transfer-print technique. *IEEE Electron Device Lett.* **2021**, *42*, 509–512. [CrossRef]
208. Watahiki, T.; Yuda, Y.; Furukawa, A.; Yamamuka, M.; Takiguchi, Y.; Miyajima, S. Heterojunction p-Cu_2O/n-Ga_2O_3 diode with high breakdown voltage. *Appl. Phys. Lett.* **2017**, *111*, 222104. [CrossRef]
209. Wang, X.; Li, M.; He, M.; Lu, H.; Chen, C.-Z.; Jiang, Y.; Wen, K.; Du, F.; Zhang, Y.; Deng, C.; et al. Optimization of CuO_x/Ga_2O_3 Heterojunction Diodes for High-Voltage Power Electronics. *Nanomaterials* **2025**, *15*, 87. [CrossRef]
210. Ghosh, S.; Baral, M.; Kamparath, R.; Choudhary, R.J.; Phase, D.M.; Singh, S.D.; Ganguli, T. Epitaxial growth and interface band alignment studies of all oxide α-Cr_2O_3/β-Ga_2O_3 pn heterojunction. *Appl. Phys. Lett.* **2019**, *115*, 061602. [CrossRef]
211. Lu, X.; Zhou, X.; Jiang, H.; Ng, K.W.; Chen, Z.; Pei, Y.; Lau, K.M.; Wang, G. 1-kV Sputtered p-NiO/n-Ga_2O_3 Heterojunction Diodes with an Ultra-Low Leakage Current Below 1μ A/cm^2. *IEEE Electron Device Lett.* **2020**, *1*, 449–452. [CrossRef]
212. Gong, H.H.; Chen, X.H.; Xu, Y.; Ren, F.-F.; Gu, S.L.; Ye, J.D. A 1.86-kV double-layered NiO/β-Ga_2O_3 vertical p-n heterojunction diode. *Appl. Phys. Lett.* **2020**, *117*, 022104. [CrossRef]
213. Liu, D.; Zhang, Z.; Chen, H.; Tian, X.; Wang, Y.; Yan, Y.; Zeng, L.; Liu, X.; Chen, D.; Feng, Q.; et al. Performance Enhancement of NiO_x/β-Ga_2O_3 Heterojunction Diodes by Synergistic Interface Engineering. *IEEE Trans. Electron Devices* **2024**, *71*, 4578–4583. [CrossRef]
214. Zhou, F.; Gong, H.; Xu, W.; Yu, X.; Xu, Y.; Yang, Y.; Ren, F.F.; Gu, S.; Zheng, Y.; Zhang, R.; et al. 1.95-kV beveled-mesa NiO/β-Ga_2O_3 heterojunction diode with 98.5% conversion efficiency and over million-times overvoltage ruggedness. *IEEE Trans. Power Electron.* **2021**, *37*, 1223–1227. [CrossRef]
215. Zhou, F.; Gong, H.H.; Wang, Z.P.; Xu, W.Z.; Yu, X.X.; Yang, Y.; Ren, F.F.; Gu, S.L.; Zhang, R.; Zheng, Y.D.; et al. Over 1.8 GW/cm^2 beveled-mesa NiO/β-Ga_2O_3 heterojunction diode with 800 V/10 A nanosecond switching capability. *Appl. Phys. Lett.* **2021**, *119*, 262103. [CrossRef]
216. Li, J.S.; Chiang, C.C.; Xia, X.; Yoo, T.J.; Ren, F.; Kim, H.; Pearton, S.J. Demonstration of 4.7 kV breakdown voltage in NiO/β-Ga_2O_3 vertical rectifiers. *Appl. Phys. Lett.* **2022**, *121*, 042105. [CrossRef]
217. Liao, C.; Lu, X.; Xu, T.; Fang, P.; Deng, Y.; Luo, H.; Wu, Z.; Chen, Z.; Liang, J.; Pei, Y.; et al. Optimization of NiO/β-Ga_2O_3 heterojunction diodes for high-power application. *IEEE Trans. Electron Devices* **2022**, *69*, 5722–5727. [CrossRef]
218. Han, T.; Wang, Y.; Lv, Y.; Dun, S.; Liu, H.; Bu, A.; Feng, Z. 2.83-kV double-layered NiO/β-Ga_2O_3 vertical pn heterojunction diode with a power figure-of-merit of 5.98 GW/cm^2. *J. Semicond.* **2023**, *44*, 072802. [CrossRef]
219. Li, J.-S.; Chiang, C.-C.; Xia, X.; Tsai, C.-T.; Ren, F.; Liao, Y.-T.; Pearton, S.J. Dynamic switching of 1.9 A/1.76 kV forward current NiO/β-Ga_2O_3 rectifiers. *ECS J. Solid State Sci. Technol.* **2022**, *11*, 105003. [CrossRef]
220. Wan, J.; Wang, H.; Cheng, H.; Wang, C.; Que, Q.; Li, Y.; Zhang, C.; Sun, J.; Liu, D.; Sheng, K. 2kV Low Leakage Vertical NiO/β-Ga_2O_3 Hetero-Junction Diode and its Thermal/Electrical Stability. In Proceedings of the 2024 36th International Symposium on Power Semiconductor Devices and ICs (ISPSD), Bremen, Germany, 2–6 June 2024; pp. 200–203.
221. Han, J.; Sun, N.; Pei, X.; Wang, R.; Fan, K.; Zhu, R.; Wang, M.; Zhu, X.; Li, X.; Li, J.; et al. 3.0 kV β-Ga_2O_3-Based Vertical pn Heterojunction Diodes with Helium-Implanted Edge Termination. *IEEE Trans. Electron Devices* **2025**, *72*, 2879–2883.

222. Li, J.-S.; Wan, H.-H.; Chiang, C.-C.; Yoo, T.J.; Ren, F.; Kim, H.; Pearton, S.J. NiO/Ga_2O_3 vertical rectifiers of 7 kV and 1 mm^2 with 5.5 A forward conduction current. *Crystals* **2023**, *13*, 1624. [CrossRef]
223. Wang, Y.; Gong, H.; Lv, Y.; Fu, X.; Dun, S.; Han, T.; Liu, H.; Zhou, X.; Liang, S.; Ye, J.; et al. 2.41 kV vertical P-Nio/n-Ga_2O_3 heterojunction diodes with a record Baliga's figure-of-merit of 5.18 GW/cm^2. *IEEE Trans. Power Electron.* **2021**, *37*, 3743–3746. [CrossRef]
224. Li, J.S.; Chiang, C.C.; Xia, X.; Wan, H.H.; Ren, F.; Pearton, S.J. Effect of drift layer doping and NiO parameters in achieving 8.9 kV breakdown in 100µm diameter and 4kV/4 A in 1 mm diameter NiO/β-Ga_2O_3 rectifiers. *J. Vac. Sci. Technol. A* **2023**, *41*, 043404. [CrossRef]
225. Li, J.-S.; Chiang, C.-C.; Xia, X.; Wan, H.-H.; Ren, F.; Pearton, S.J. 1 mm^2, 3.6 kV, 4.8 A NiO/Ga_2O_3 heterojunction rectifiers. *ECS J. Solid State Sci. Technol.* **2023**, *12*, 085001. [CrossRef]
226. Li, J.-S.; Wan, H.-H.; Chiang, C.-C.; Xia, X.; Yoo, T.J.; Kim, H.; Ren, F.; Pearton, S.J. Reproducible NiO/Ga_2O_3 Vertical Rectifiers with Breakdown Voltage >8 kV. *Crystals* **2023**, *13*, 886. [CrossRef]
227. Hendricks, N.S.; Farzana, E.; Islam, A.E.; Leedy, K.D.; Liddy, K.J.; Williams, J.; Dryden, D.M.; Adams, A.M.; Speck, J.S.; Chabak, K.D.; et al. Vertical metal-dielectric-semiconductor diode on (001) β-Ga_2O_3 with high-k TiO_2 interlayer exhibiting reduced turn-on voltage and leakage current and improved breakdown. *Appl. Phys. Express* **2023**, *16*, 071002. [CrossRef]
228. Xu, M.; Biswas, A.; Li, T.; He, Z.; Luo, S.; Mei, Z.; Zhou, J.; Chang, C.; Puthirath, A.B.; Vajtai, R.; et al. Vertical β-Ga_2O_3 metal-nsulator-semiconductor diodes with an ultrathin boron nitride interlayer. *Appl. Phys. Lett.* **2023**, *123*, 232107.
229. Lv, Y.; Wang, Y.; Fu, X.; Dun, S.; Sun, Z.; Liu, H.; Zhou, X.; Song, X.; Dang, K.; Liang, S.; et al. Demonstration of β-Ga_2O_3 Junction Barrier Schottky Diodes with a Baliga's Figure of Merit of 0.85 GW/cm^2 or a 5 A/700 V Handling Capabilities. *IEEE Trans. Power Electron.* **2021**, *36*, 6179–6182. [CrossRef]
230. Yan, Q.; Gong, H.; Zhang, J.; Ye, J.; Zhou, H.; Liu, Z.; Xu, S.; Wang, C.; Hu, Z.; Feng, Q.; et al. β-Ga_2O_3 hetero-junction barrier Schottky diode with reverse leakage current modulation and $BV^2/R_{on,sp}$ value of 0.93 GW/cm^2. *Appl. Phys. Lett.* **2021**, *118*, 122102. [CrossRef]
231. Zhang, F.; Zheng, X.; He, Y.; Wang, X.; Hong, Y.; Zhang, X.; Yuan, Z.; Wang, Y.; Lu, X.; Yin, J.; et al. The Impact of Anode p+ Islands Layout on the Performance of NiO_x/β-Ga_2O_3 Hetero-Junction Barrier Schottky Diodes. *IEEE Trans. Electron Devices* **2023**, *70*, 5603–5608. [CrossRef]
232. Wang, J.; Yao, X.-W.; Xu, X.-X.; Wu, X.; Qian, J.-H.; Wang, X.-J.; Liu, Y.-F.; Wu, C.-Y.; Luo, L.-B. SnO/β-Ga_2O_3 heterojunction barrier Schottky diodes for decreased reverse leakage current and improved breakdown voltage. *J. Mater. Chem. C* **2025**, *13*, 9992–9996. [CrossRef]
233. Hu, T.C.; Wang, Z.P.; Sun, N.; Gong, H.H.; Yu, X.X.; Ren, F.F.; Yang, Y.; Gu, S.L.; Zheng, Y.D.; Zhang, R.; et al. A self-aligned Ga_2O_3 heterojunction barrier Schottky power diode. *Appl. Phys. Lett.* **2023**, *123*, 013507. [CrossRef]
234. Gong, H.H.; Yu, X.X.; Xu, Y.; Chen, X.H.; Kuang, Y.; Lv, Y.J.; Yang, Y.; Ren, F.F.; Feng, Z.H.; Gu, S.L.; et al. β-Ga_2O_3 vertical heterojunction barrier Schottky diodes terminated with p-NiO field limiting rings. *Appl. Phys. Lett.* **2021**, *118*, 202102. [CrossRef]
235. Wei, J.; Wei, Y.; Lu, J.; Peng, X.; Jiang, Z.; Yang, K.; Luo, X. Experimental study on electrical characteristics of large-size vertical β-Ga_2O_3 junction barrier Schottky diodes. In Proceedings of the 2022 IEEE 34th International Symposium on Power Semiconductor Devices and ICs (ISPSD), Vancouver, BC, Canada, 22–25 May 2022; pp. 97–100.
236. Hu, Z.; Zhou, H.; Dang, K.; Cai, Y.; Feng, Z.; Gao, Y.; Feng, Q.; Zhang, J.; Hao, Y. Lateral β-Ga_2O_3 Schottky Barrier Diode on Sapphire Substrate with Reverse Blocking Voltage of 1.7 kV. *IEEE J. Electron Devices Soc.* **2018**, *6*, 815–820. [CrossRef]
237. Hu, Z.; Zhou, H.; Feng, Q.; Zhang, J.; Zhang, C.; Dang, K.; Cai, Y.; Feng, Z.; Gao, Y.; Kang, X.; et al. Field-Plated Lateral β-Ga_2O_3 Schottky Barrier Diode with High Reverse Blocking Voltage of More Than 3 kV and High DC Power Figure-of-Merit of 500 MW/cm^2. *IEEE Electron Device Lett.* **2018**, *39*, 1564–1567. [CrossRef]
238. Wang, C.; Yan, Q.; Zhang, C.; Su, C.; Zhang, K.; Sun, S.; Liu, Z.; Zhang, W.; Alghamdi, S.; Ghandourah, E.; et al. β-Ga_2O_3 lateral Schottky barrier diodes with >10 kV breakdown voltage and anode engineering. *IEEE Electron Device Lett.* **2023**, *44*, 1684–1687. [CrossRef]
239. Roy, S.; Bhattacharyya, A.; Peterson, C.; Krishnamoorthy, S. β-Ga_2O_3 Lateral High-Permittivity Dielectric Superjunction Schottky Barrier Diode With 1.34 GW/cm^2 Power Figure of Merit. *IEEE Electron Device Lett.* **2022**, *43*, 2037–2040. [CrossRef]
240. Qin, Y.; Xiao, M.; Porter, M.; Ma, Y.; Spencer, J.; Du, Z.; Jacobs, A.G.; Sasaki, K.; Wang, H.; Tadjer, M.; et al. 10-kV Ga_2O_3 charge-balance Schottky rectifier operational at 200 °C. *IEEE Electron Device Lett.* **2023**, *44*, 1268–1271. [CrossRef]
241. Cho, K.J.; Chang, W.; Lee, H.-K.; Mun, J.K. β-Ga_2O_3 schottky barrier diodes with near-zero turn-on voltage and breakdown voltage over 3.6 kV. *Trans. Electr. Electron. Mater.* **2024**, *25*, 365–369. [CrossRef]
242. Khan, D.; Gajula, D.; Okur, S.; Tompa, G.S.; Koley, G. β-Ga_2O_3 thin film based lateral and vertical Schottky barrier diode. *ECS J. Solid State Sci. Technol.* **2019**, *8*, Q106. [CrossRef]
243. Xu, Y.; Chen, X.; Cheng, L.; Ren, F.-F.; Zhou, J.; Bai, S.; Lu, H.; Gu, S.; Zhang, R.; Zheng, Y.; et al. High performance lateral Schottky diodes based on quasi-degenerated Ga_2O_3. *Chin. Phys. B* **2019**, *28*, 038503. [CrossRef]

244. Liu, Q.; Zhou, X.; He, Q.; Hao, W.; Zhao, X.; Hua, M.; Xu, G.; Long, S. Demonstration of β-Ga_2O_3 heterojunction gate field-effect rectifier. *IEEE Trans. Electron Devices* **2023**, *70*, 3762–3767. [CrossRef]
245. Zhang, D.; Chen, H.; He, W.; Hong, Z.; Lu, Q.; Guo, L.; Liu, T.; Liu, X.; Hao, Y. Characteristic of flexible β-Ga_2O_3 Schottky barrier diode based on mechanical stripping process. *Superlattices Microstruct.* **2021**, *160*, 107078. [CrossRef]
246. Hao, W.; Wu, F.; Li, W.; Xu, G.; Xie, X.; Zhou, K.; Guo, W.; Zhou, X.; He, Q.; Zhao, X.; et al. Improved vertical β-Ga_2O_3 Schottky barrier diodes with conductivity-modulated p-NiO junction termination extension. *IEEE Trans. Electron Devices* **2023**, *70*, 2129–2134. [CrossRef]
247. Wang, B.; Xiao, M.; Spencer, J.; Qin, Y.; Sasaki, K.; Tadjer, M.J.; Zhang, Y. 2.5 kV vertical Ga_2O_3 Schottky rectifier with graded junction termination extension. *IEEE Electron Device Lett.* **2023**, *44*, 221–224. [CrossRef]
248. Xiao, M.; Wang, B.; Spencer, J.; Qin, Y.; Porter, M.; Ma, Y.; Wang, Y.; Sasaki, K.; Tadjer, M.; Zhang, Y. NiO junction termination extension for high-voltage (>3 kV) Ga_2O_3 devices. *Appl. Phys. Lett.* **2023**, *122*, 183501. [CrossRef]
249. Hong, Y.; Zheng, X.; He, Y.; Zhang, H.; Zhang, W.; Zhang, J.; Ma, X.; Hao, Y. Effect of p-NiO_x junction termination extension on interface states in NiO_x/ β-Ga_2O_3 heterojunction diodes. *Mater. Sci. Semicond. Process.* **2025**, *185*, 108987. [CrossRef]
250. Gilankar, A.; Katta, A.; Das, N.; Kalarickal, N.K. >3kV NiO/Ga_2O_3 Heterojunction Diodes with Space-Modulated Junction Termination Extension and Sub-1V Turn-on. *IEEE J. Electron Devices Soc.* **2025**, *13*, 373–377. [CrossRef]
251. Liu, M.; Gao, H.; Tian, X.; Cai, Y.; Feng, Q.; Liu, C.; Zhang, C.; Zhang, J.; Hao, Y. Vertical β-Ga_2O_3 Schottky Barrier Diode with the Composite Termination Structure. *ECS J. Solid State Sci. Technol.* **2024**, *13*, 125001. [CrossRef]
252. Gong, H.; Sun, N.; Hu, T.; Yu, X.; Porter, M.; Yang, Z.; Ren, F.; Gu, S.; Zheng, Y.; Zhang, R.; et al. Ga_2O_3/NiO junction barrier Schottky diodes with ultra-low barrier TiN contact. *Appl. Phys. Lett.* **2024**, *124*, 233507. [CrossRef]
253. Han, Z.; Hao, W.; Liu, J.; Xu, G.; Hu, Q.; Zheng, Z.; Yang, S.; Long, S. Improved β-Ga_2O_3 Schottky Barrier Diodes Featuring p-NiO Gradual Junction Termination Extension within Mesa Structure. In Proceedings of the 2024 36th International Symposium on Power Semiconductor Devices and ICs (ISPSD), Bremen, Germany, 2–6 June 2024; pp. 232–235.
254. Prajapati, P.; Lodha, S. Barrier height enhancement in β-Ga_2O_3 Schottky diodes using an oxygen-rich ultra-thin AlO_x interfacial layer. *Appl. Phys. Lett.* **2024**, *125*, 061602. [CrossRef]
255. Qin, Y.; Porter, M.; Xiao, M.; Du, Z.; Zhang, H.; Ma, Y.; Spencer, J.; Wang, B.; Song, Q.; Sasaki, K.; et al. 2 kV, 0.7 $m\Omega\cdot cm^2$ Vertical Ga_2O_3 Superjunction Schottky Rectifier with Dynamic Robustness. In Proceedings of the 2023 International Electron Devices Meeting (IEDM), San Francisco, CA, USA, 9–13 December 2023; pp. 1–4.
256. Hendricks, N.S.; Islam, A.E.; Sowers, E.A.; Williams, J.; Dryden, D.M.; Liddy, K.J.; Wang, W.; Speck, J.S.; Green, A.J. Current transport mechanisms of metal/TiO_2/β-Ga_2O_3 diodes. *J. Appl. Phys.* **2024**, *135*, 095705. [CrossRef]
257. Li, M.; He, M.; Wang, X.; Jiang, Y.; Wen, K.; Du, F.; Deng, C.; He, J.; Zhang, Y.; Yu, W.; et al. High-performance β-Ga_2O_3 Schottky barrier diodes with Mg current blocking layer using spin-on-glass technique. *Appl. Phys. Lett.* **2024**, *125*, 132101. [CrossRef]